Neuroprotective intervention by interferon-γ blockade prevents CD8+ T cell–mediated dendrite and synapse loss

Mario Kreutzfeldt,[1,3] Andreas Bergthaler,[1,2,4] Marylise Fernandez,[1,2] Wolfgang Brück,[5] Karin Steinbach,[1,3] Mariann Vorm,[5] Roland Coras,[6] Ingmar Blümcke,[6] Weldy V. Bonilla,[1,2] Anne Fleige,[7] Ruth Forman,[8] Werner Müller,[8] Burkhard Becher,[9] Thomas Misgeld,[10,11,13] Martin Kerschensteiner,[12,13] Daniel D. Pinschewer,[1,2] and Doron Merkler[1,3,5]

[1]Department of Pathology and Immunology and [2]World Health Organization Collaborating Centre for Vaccine Immunology, University of Geneva, 1211 Geneva, Switzerland
[3]Division of Clinical Pathology, Geneva University Hospital, 1211 Geneva, Switzerland
[4]CeMM Research Center for Molecular Medicine of the Austrian Academy of Sciences, 1090 Vienna, Austria
[5]Department of Neuropathology, Georg-August-University Goettingen, 37099 Goettingen, Germany
[6]Department of Neuropathology, University Hospital Erlangen, 91054 Erlangen, Germany
[7]Helmholtz Centre for Infection Research, Department of Experimental Immunology, University of Braunschweig, 38124 Braunschweig, Germany
[8]Faculty of Life Sciences, University of Manchester, Manchester M13 9PT, England, UK
[9]Institute of Experimental Immunology, University of Zurich, 8057 Zurich, Switzerland
[10]Institute of Neuronal Cell Biology, Technische Universität München, 80802 Munich, Germany
[11]German Center for Neurodegenerative Diseases (DZNE), 80336 Munich, Germany
[12]Institute of Clinical Neuroimmunology, Ludwig-Maximilians University Munich, 81377 Munich, Germany
[13]Munich Cluster for Systems Neurology (SyNergy), 80336 Munich, Germany

Neurons are postmitotic and thus irreplaceable cells of the central nervous system (CNS). Accordingly, CNS inflammation with resulting neuronal damage can have devastating consequences. We investigated molecular mediators and structural consequences of CD8+ T lymphocyte (CTL) attack on neurons in vivo. In a viral encephalitis model in mice, disease depended on CTL-derived interferon-γ (IFN-γ) and neuronal IFN-γ signaling. Downstream STAT1 phosphorylation and nuclear translocation in neurons were associated with dendrite and synapse loss (deafferentation). Analogous molecular and structural alterations were also found in human Rasmussen encephalitis, a CTL-mediated human autoimmune disorder of the CNS. Importantly, therapeutic intervention by IFN-γ blocking antibody prevented neuronal deafferentation and clinical disease without reducing CTL responses or CNS infiltration. These findings identify neuronal IFN-γ signaling as a novel target for neuroprotective interventions in CTL-mediated CNS disease.

CORRESPONDENCE
D. Merkler:
doron.merkler@unige.ch

Abbreviations used: CNS, central nervous system; DCN, deep cerebellar nuclei; i.c., intracranial; IFNGR, IFN-γ receptor; LCMV, lymphocytic choriomeningitis virus; MAP-2, microtubule-associated protein 2; MS, multiple sclerosis; RE, Rasmussen's encephalitis.

In many inflammatory diseases of the central nervous system (CNS) neuronal damage determines permanent neurological deficits. Novel strategies for neuroprotection are urgently sought and require a detailed understanding of the mechanisms underlying neuronal damage. The key contribution of cytotoxic CD8+ T lymphocytes (CTLs) to this process has become increasingly appreciated in recent years (Neumann et al., 2002). CTLs are commonly recruited to the brain in viral infections, paraneoplastic disorders (Albert and Darnell, 2004), and autoimmune diseases such as multiple sclerosis (MS) and Rasmussen's encephalitis (RE; Hauser et al., 1986; Bien et al., 2005; Friese and Fugger, 2005; Goverman, 2009). Upon engagement of their cognate peptide–MHC class I (MHC-I) complex on target cells, CTLs activate an array of effector functions. Cytotoxicity is

M. Kreutzfeldt and A. Bergthaler contributed equally to this paper.
D.D. Pinschewer and D. Merkler contributed equally to this paper.

The Rockefeller University Press $30.00
J. Exp. Med. 2013 Vol. 210 No. 10 2087-2103
www.jem.org/cgi/doi/10.1084/jem.20122143

The Journal of Experimental Medicine

typically mediated by perforin-dependent mechanisms and Fas–FasL (CD95/CD95L) interactions (Stinchcombe and Griffiths, 2007), but CTLs also secrete cytokines including IFN-γ and TNF. The relative contribution of each of these pathways to tissue damage varies greatly and depends on the target cell type and tissue (Guidotti et al., 1996; Kägi et al., 1996; Medana et al., 2000). At the same time, CTL cytotoxicity and cytokine secretion can also both contribute to virus control in the CNS (Binder and Griffin, 2001; Shrestha and Diamond, 2007; Pinschewer et al., 2010b).

Neurons show limited turnover and regenerative capacity yet serve essential functions. Classical concepts have therefore suggested that neurons are spared from CTL attack. This "immune privilege" has been accredited to limited MHC-I expression (Joly et al., 1991), secretion of immunomodulatory TGF-β (Liu et al., 2006), and expression of Fas-L (Medana et al., 2001a). The same mechanisms are also thought to represent an evolutionary reason why neurons serve as a sanctuary for several RNA and DNA viruses, namely members of the *Herpes*, *Paramyxo*-, and *Arenavirus* families (Brown et al., 1979; Sequiera et al., 1979; ter Meulen et al., 1984; Joly et al., 1991). Recent studies have shown, however, that infected neurons do not escape CTL recognition altogether (McDole et al., 2010). For example, CNS-infiltrating CTLs established stable peptide/MHC-I–specific contacts with Herpes simplex virus– or Borna disease virus–infected neurons, respectively (Khanna et al., 2003; Chevalier et al., 2011). In the Theiler's murine encephalomyelitis virus model, depletion of CTLs or genetic deficiency in MHC-I or perforin preserved axon integrity and prevented neurological deficits (Murray et al., 1998; Deb et al., 2009, 2010). CTLs can attack neuronal somata (Manning et al., 1987) and axons (Medana et al., 2001b) in primary neuronal cultures and explants, and cultured neurons are sensitive to lysis or silencing by perforin (Rensing-Ehl et al., 1996; Meuth et al., 2009). The Fas/Fas-L pathway can cause cytoskeleton breaks and membrane disruption which eventually cause neuronal death (Medana et al., 2000). However, the morphology, electrical activity, and glial cell environment of neurons differ considerably between in vitro culture conditions and the natural tissue habitat, and all of these factors can affect susceptibility to CTL attack (Neumann et al., 1995). Hence, we still lack a clear understanding of how CTLs damage neurons in vivo and which alterations result from such damage.

We have recently established the viral déjà vu model, allowing us to study CTL-mediated neuronal damage and the resulting disease in vivo (Merkler et al., 2006). Neonatal intracranial (i.c.) infection of mice with an attenuated lymphocytic choriomeningitis virus (LCMV) variant (rLCMV/INDG) results in viral persistence selectively in CNS neurons (a status referred to as carrier mice). rLCMV/INDG is not cytolytic and carrier mice are therefore clinically healthy, but they express viral nonself-antigens in neurons. Notably, they are free of CNS-infiltrating T cells, and viral epitope-specific $CD8^+$ T cell frequencies in peripheral blood remain below detection limits of peptide/MHC-I tetramer measurements (Merkler et al., 2006). This indicates that neonatal rLCMV/INDG infection fails to trigger a clinically significant CTL response. Upon adult infection with LCMV WT (LCMVwt; referred to as challenge), carrier mice mount vigorous CTL responses against the immunodominant H-$2D^b$–restricted nucleoprotein-derived epitope NP396 that is shared between rLCMV/INDG and LCMVwt. These CTLs infiltrate the CNS gray matter, attack NP396-expressing rLCMV/INDG-infected neurons, and cause severe disease within 7–10 d after challenge. The topographical distribution and the composition of inflammatory infiltrates in viral déjà vu disease recreate histopathological hallmarks of RE. In this human autoimmune disease, oligoclonal and therefore putatively antigen-specific $CD8^+$ T cell populations dominate the histological picture and are typically found in direct contact with neurons (Li et al., 1997; Bien et al., 2005). The clinical presentation of RE is characterized by treatment-refractory epilepsy with consequent intellectual decline and hemiparesis, thus necessitating surgical resection of affected brain regions. A viral contribution to RE pathogenesis has long been suspected but remains to be substantiated (Friedman et al., 1977; Walter and Renella, 1989; Farrell et al., 1991).

Here, we show that CTL attack on neurons in vivo induces rapid loss of dendrites and synapses rather than neuronal depletion. This deafferentation and the resulting disease depend on IFN-γ signaling from CTLs to neurons but neither on Fas- nor on perforin-dependent pathways. Accordingly, STAT1 phosphorylation and nuclear translocation together with deafferentation represented hallmarks of both the murine viral déjà vu model and human RE. These findings provide important new insights into the molecular mechanisms and cellular consequences of CTL–neuron interactions in viral and autoimmune CNS disorders. This delineates a promising new strategy for neuroprotective intervention in immune-mediated CNS disease.

RESULTS

CTLs mediate deafferentation of antigenic neurons in vivo

We set out to investigate molecular pathways as well as morphological and clinical consequences of CTL attack on neurons. The viral déjà vu model is characterized by CTL infiltrates in the cerebral cortex, basal ganglia, thalamic and hypothalamic nuclei, hippocampus, cerebellum, brain stem, and some segments of the spinal cord (Merkler et al., 2006). First, we assessed whether neuronal loss could account for the acute clinical impairment, which starts at day 7–10 after challenge and includes ataxia, locomotor dysfunction, and occasional paroxysmal seizures. 3 wk after challenge, thus, 2 wk after disease onset, neuronal cell densities remained unaltered in all anatomical areas under study (Fig. 1). In contrast, tissue collected another 5 wk later displayed a minor yet significant reduction of neuronal densities in brain stem, spinal cord, and hypothalamus but not in cortex dentate gyrus. Thus, albeit a consistent finding in later stages, irreversible neuronal drop-out was unlikely to cause the rapidly developing and severe neurological impairments peaking at day 10 after challenge.

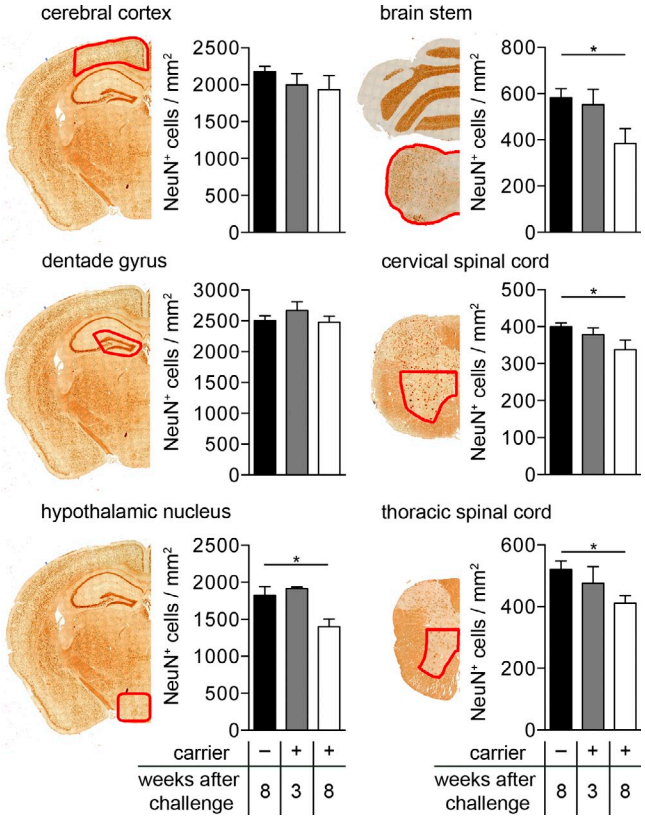

Figure 1. Neuronal loss is observed in late stages of viral déjà vu disease. Adult carrier mice (+) and noncarrier controls (−) were subject to challenge (day 0) with LCMVwt (10^4 PFU) i.v. 3 or 8 wk later, neuronal density (NeuN⁺) was quantified in various brain and spinal cord areas as indicated in the graph. NeuN⁺ cells within these areas were detected using a computerized algorithm and expressed as cells per square millimeter. The anatomical areas under study are delimited by red lines, which were drawn according to anatomical landmarks. Error bars represent the mean + SEM of 4–12 mice per anatomical area and group. Shown are pooled data from two independent experiments. *, $P < 0.05$.

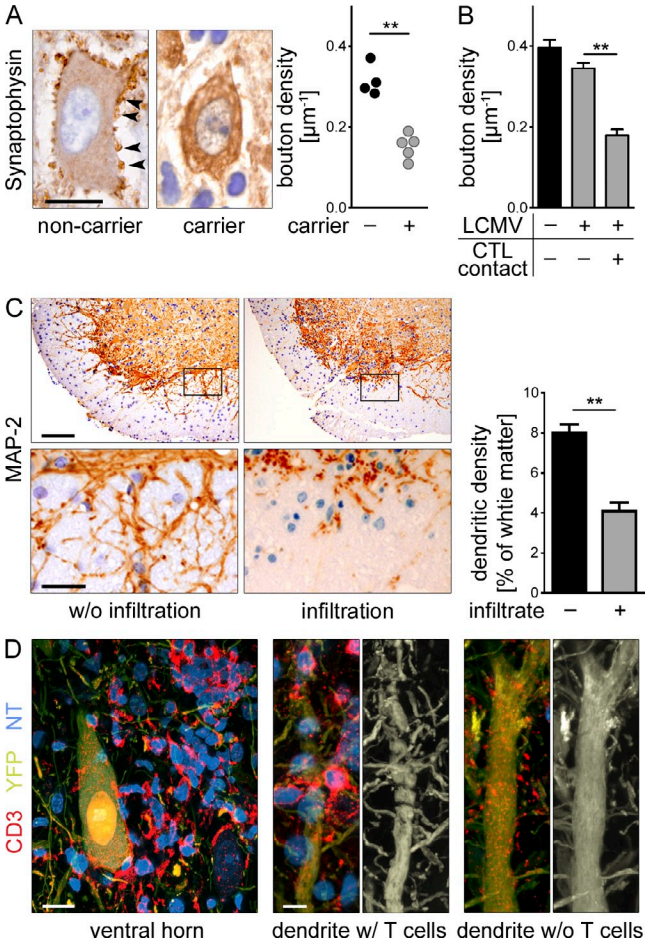

Figure 2. Deafferentation in viral déjà vu disease requires CTL contact with infected neurons. (A–D) Carrier mice (C57BL/6 WT or YFP reporter mice) and noncarrier controls (without neonatal infection) were challenged with LCMVwt (10^4 PFU) i.v. in adulthood. (A) 10 d later, animals were sacrificed and brains were processed for histological analysis Left: representative section stained for synaptophysin⁺ perisomatic boutons (arrowheads) in the DCN of carrier and noncarrier mice 10 d after challenge. Right: quantification of perisomatic bouton density. Symbols represent individual animals. (B) On day 8 after challenge, CNS sections of DCN were triple immunostained for T cells, synaptophysin, and LCMV-NP antigen ($n = 4$ animals). Perisomatic bouton density was quantified in LCMV-NP–positive (+) neurons that were in juxtaposition to infiltrating T cells. (C) Dendritic projections into the spinal cord white matter in inflamed and noninflamed areas were quantified on MAP-2–immunostained sections ($n = 4$). (D) T cell infiltrates (CD3⁺, red) in the spinal cord of YFP-H mice (yellow subset of neurons). Proximity of T cells to somata of ventral horn neurons (left) and dendrites (middle) is shown. Dendrites without neighboring T cells (right) are also shown. Monochromatic YFP images (middle and right only) illustrate dendrite morphology. Nuclei were visualized with neurotrace (NT). Error bars in B and C represent the mean + SEM of 4 mice per group. Bars: (A) 20 µm; (C, top) 200 µm; (C, bottom) 50 µm; (D, left) 20 µm; (D, middle and right) 10 µm. One representative dataset out of two similar experiments is shown for A–D. **, $P < 0.01$.

We hypothesized that neuronal integration into synaptic networks rather than viability may be impaired as a result of CTL attack. Thus, we analyzed the density of dendrites on spinal cord motor neurons and counted perisomatic presynaptic boutons on neurons in the deep cerebellar nuclei (DCN). These anatomical areas represent components of important functional networks, display well defined cytological features (Garin and Escher, 2001), and can also be affected in human inflammatory CNS diseases (Dalmau and Rosenfeld, 2008; Gilmore et al., 2009). In healthy noncarrier controls, the somata of DCN were surrounded by so-called perisomatic boutons, i.e., punctate synaptophysin-positive areas corresponding to putative synapses (Fig. 2 A). In contrast, the number of such boutons was significantly reduced in virus carriers with viral déjà vu disease. Such a reduction was preferentially observed on neurons, which expressed LCMV-NP—i.e., were antigenic targets for pathogenic CTLs—and were in direct contact with one or more T cells (Fig. 2 B). This suggested that perisomatic boutons were lost as a consequence of an epitope-specific targeted CTL attack. Conversely, the inflammatory milieu to which neighboring neurons (without direct CTL contact) were exposed in a "bystander" fashion was apparently much less able to induce the observed alterations.

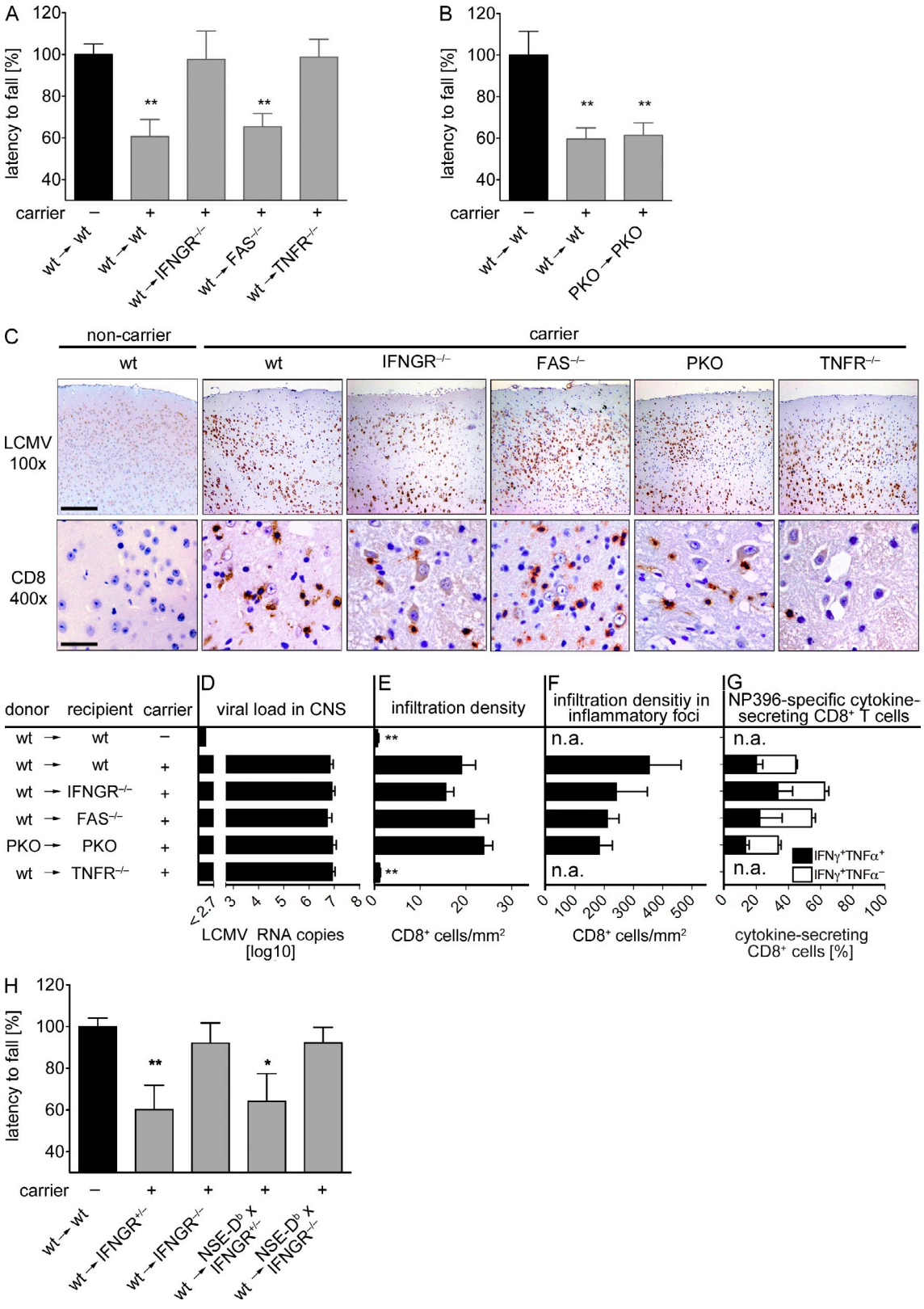

Figure 3. Viral déjà vu disease depends on nonhematopoietic IFNGR but neither on Fas nor on perforin. Adult carrier mice and noncarrier controls of the indicated genotypes were lethally irradiated and reconstituted with WT or perforin-deficient (PKO) bone marrow cells. Subsequently, mice were challenged with LCMVwt (10^4 PFU) i.v. Rotarod performance (A, B, and H), tissues, and brain-infiltrating CTLs (C–G) were analyzed at the peak of disease (day 10 after challenge). (A) Error bars represent the mean + SEM of 19–31 mice per group. (B) As a modification to the setup in A, all groups of mice were

Neurons not only receive afferent input at perisomatic synapses but mostly via their dendrites. Microtubule-associated protein 2 (MAP-2) is expressed in neuronal somata and dendrites (Johnson and Jope, 1992) and marks bundles of dendrites, which project into the ventro-lateral white matter of the spinal cord. Spinal cord segments that were diffusely infiltrated by CTLs exhibited significantly reduced dendrite densities (Fig. 2 C). Confocal microscopic analysis of fluorescently labeled neurons (*Thy1*-YFP-H reporter mice (Feng et al., 2000; Fig. 2 D) revealed that dendritic fragmentation was typically found in close spatial association with infiltrating T cells. Such neuronal deafferentation—rather than neuronal loss—occurred concomitantly with the early manifestations of viral déjà vu disease, thus representing a likely structural correlate thereof.

Nonhematopoietic IFN-γ receptors (IFNGRs), but neither Fas nor perforin, are necessary for viral déjà vu disease and neuronal deafferentation

Next, we analyzed the individual contribution of the CTL effector pathways FAS, perforin, IFN-γ, and TNF to disease manifestation. Defective Fas-, IFN-γ, or TNF signaling can hamper the induction, expansion, or maturation of CTLs (Watanabe-Fukunaga et al., 1992; Whitmire et al., 2005; Kim et al., 2006). Hence, we relied on bone marrow chimeric mice to perform these studies. Viral carriers lacking TNF receptors 1 and 2 (TNFR1/2$^{-/-}$), Fas (FAS$^{-/-}$), or IFNGR$^{-/-}$ and WT controls were lethally irradiated and reconstituted with WT bone marrow, such that the immune system was of WT origin, but the respective receptor defects persisted in nonlymphohematopoietic cells of the CNS. Both WT→IFNGR$^{-/-}$ and WT→TNFR1/2$^{-/-}$ were protected from viral déjà vu disease, indicating that IFN-γ and TNF signaling in the CNS were necessary to precipitate neurological impairment (Fig. 3 A). In contrast, mice lacking FAS signaling (WT→FAS$^{-/-}$) in the CNS showed unaltered susceptibility to viral déjà vu disease. Unlike the above receptor–ligand interactions, perforin-dependent cytotoxicity operates independently of a cellular receptor but is generally considered a key effector mechanism of CTLs. A separate set of experiments established, however, that perforin deficiency did not affect disease manifestation either (Fig. 3 B). Differences in virus loads or CD8$^+$ T cell responses between groups could have confounded the above experiments. When assessing the frequency of NP396-specific CTLs in peripheral blood, we found them spread out over a similar range in all experimental groups ($P > 0.05$ for all comparisons). Differences in the magnitude of CTL responses were therefore unlikely to account for differential disease susceptibility (unpublished data). Likewise, the assessment of rLCMV/INDG distribution and RNA loads in brain did not reveal any differences between groups, which could have accounted for the resistance of WT→TNFR1/2$^{-/-}$ or WT→IFNGR$^{-/-}$ mice to disease (Fig. 3, C and D). We quantified total CD8$^+$ T cells in the CNS (Fig. 3 E) and separately also within inflammatory foci in the DCN (Fig. 3 F) where neuronal alterations were prominent (compare with Fig. 2 B). Infiltrate densities were comparable in all carrier groups, with the notable exception of WT→TNFR1/2$^{-/-}$ mice, in which CTL infiltration was virtually absent (Fig. 3, C–F). Transmigration of immune cells into the CNS requires TNF-dependent activation of the vascular endothelium (Kallmann et al., 2000), thus likely explaining the absence of CTL infiltrates in WT→TNFR1/2$^{-/-}$ carriers and resistance to disease. This prevented us from further analyzing a potential direct contribution of CTL-derived TNF to neuronal damage. Conversely, not only the number but also the functionality of brain-infiltrating CD8$^+$ T cells in WT→IFNGR$^{-/-}$ carriers was comparable to WT→WT controls, as judged by these cells' ability to produce IFN-γ and TNF (Fig. 3 G). These observations suggested that IFN-γ signaling to CNS-resident cells was essential for disease, and our previous work had documented that CNS-infiltrating CTLs associate preferentially with rLCMV/INDG-infected neurons (Merkler et al., 2006). Hence, we investigated the possibility that IFN-γ acted on neurons.

Previous in vitro studies have shown that IFN-γ can induce neuronal alterations in two distinct ways: first, IFN-γ can influence CTL–neuron interaction indirectly by up-regulating MHC-I expression on neurons and facilitate their recognition as CTL targets in vitro (Neumann et al., 1995). Second, IFN-γ can act as an effector cytokine to directly induce neuronal pathology (Kim et al., 2002). To differentiate between these two possibilities, we exploited transgenic mice, which constitutively overexpress the MHC-I molecule H-2D^b on neurons (NSE-D^b transgenic mice; Rall et al., 1995). The NP396 epitope is presented on H-2D^b and the respective CTLs drive viral déjà vu disease (Merkler et al., 2006), but constitutive H-2D^b overexpression did not restore susceptibility to viral déjà vu disease in WT→IFNGR$^{-/-}$ mice (Fig. 3 H). This suggested that IFN-γ caused disease irrespective of its role in neuronal MHC-I up-regulation.

In concordance with the clinical manifestations of disease, perisomatic bouton densities were reduced in inflammatory

given 10^4 P14xRAG splenocytes by adoptive transfer on day −1 of challenge (for details see Materials and methods). Error bars represent the mean + SEM of 4–8 mice per group. (C) Representative brain sections from the indicated experimental groups were stained for LCMV-NP antigen (top row) and infiltrating CTLs (bottom row). (D) Viral RNA load in brain was determined by TaqMan RT-PCR. Uninfected mice were tested for technical background determination. (E) Density of CD8$^+$ T cell infiltrates in brain (cerebrum and cerebellum) as determined in histopathology. (F) Density of CD8$^+$ T cell infiltrates inside inflammatory foci in DCN (not detectable in WT→TNFR1/2$^{-/-}$ mice and thus not assessed [n.a.]). Error bars in D–F represent the mean + SEM of 3–7 animals per group. (G) Cytokine profile of brain-infiltrating NP396-specific (pathogenic) CD8$^+$ T cells. Error bars show the mean + SEM of 2–4 mice per group. (H) Mice were infected and challenged as in A. Error bars represent the mean + SEM of 5–10 mice. Rotarod performance of the various experimental groups was compared with challenged WT→WT noncarrier controls. Bars: (C, top row) 200 µm; (C, bottom row) 50 µm. Shown are data pooled from five similar experiments (A), from one out of two similar experiments (B–F), or from one experiment (G and H), respectively. *, $P < 0.05$; **, $P < 0.01$.

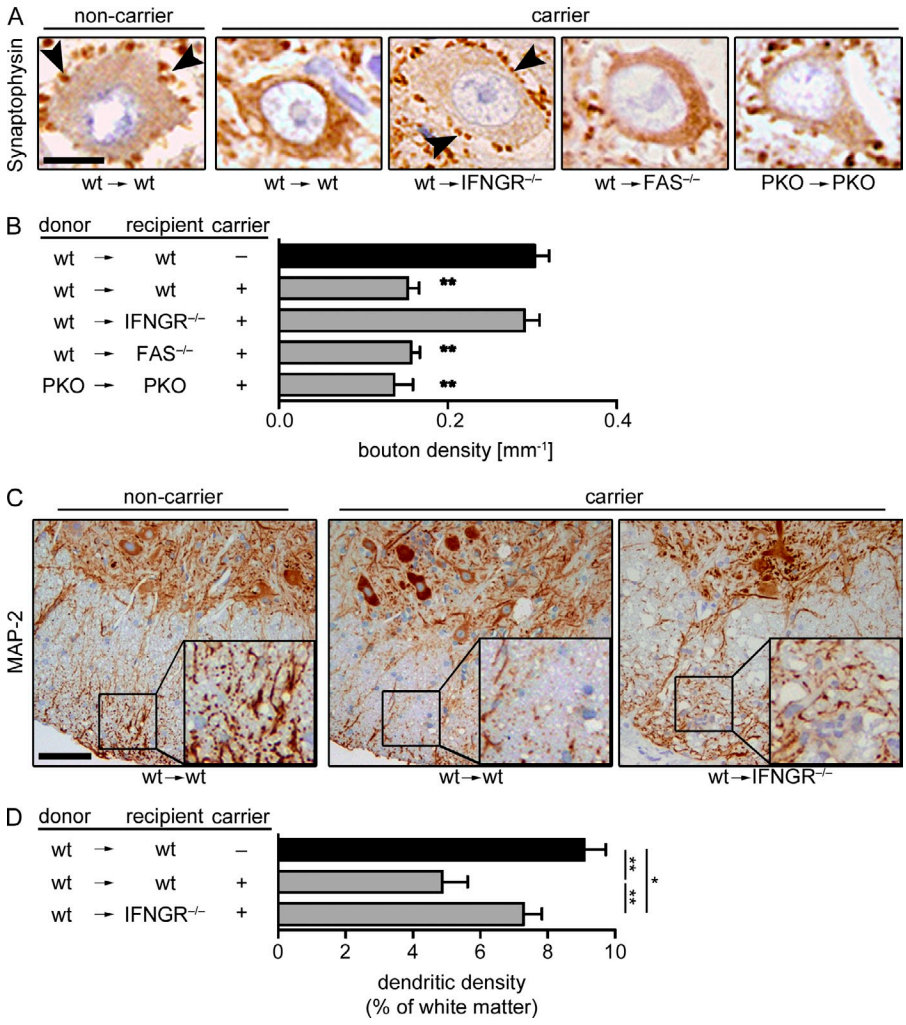

Figure 4. Deficiency in IFNGR signaling prevents perisomatic bouton loss in DCN and affords partial protection against dendritic alterations in spinal cord. Viral déjà vu experiments were conducted with bone marrow chimeric carrier mice of the indicated genotypes and carrier state. At the peak of disease (day 10) synaptophysin$^+$ perisomatic boutons on DCN neurons (A and B) and MAP-2$^+$ dendritic processes into the spinal cord white matter (C and D) were visualized by immunohistochemistry. (A) Representative picture of synaptophysin$^+$ boutons in DCN of the various experimental groups. Arrowheads indicate perisomatic boutons of WT→WT noncarrier control animals and on neurons of WT→IFNGR$^{-/-}$ mice. (B) Quantitative analysis of perisomatic bouton density in the same animals as in A. Error bars indicate the mean + SEM of 3–7 mice per group. (C) Representative pictures of spinal cord MAP-2 staining in the indicated groups. (D) Dendritic projections into the spinal cord white matter in WT→IFNGR$^{-/-}$ and WT→WT areas were quantified on MAP-2–immunostained sections. Error bars represent the mean + SEM of three to six mice per group. Bars: (A) 10 µm; (C) 50 µm. Shown are representative data from one out of two similar experiments (A–D). *, $P < 0.05$; **, $P < 0.01$.

foci of diseased WT→Fas$^{-/-}$, PKO→PKO, and WT→WT controls but remained at normal levels in resistant WT→IFNGR$^{-/-}$ carriers (Fig. 4, A and B). Likewise, dendrites of WT→IFNGR$^{-/-}$ mice remained at least partially conserved upon challenge (Fig. 4, C and D). Collectively these results identified IFN-γ signaling as a main trigger of neuronal deafferentation.

STAT1 up-regulation, phosphorylation, and nuclear translocation are hallmarks of IFN-γ signaling in neurons

We next investigated IFNGR downstream signaling by measuring expression, phosphorylation, and nuclear translocation of the transcription factor STAT1 (Ramana et al., 2002). *Stat1* mRNA was significantly up-regulated in brains of WT→WT controls with viral déjà vu disease but not in resistant WT→IFNGR$^{-/-}$ mice (Fig. 5 A). Furthermore, numerous nuclei of WT→WT but not WT→IFNGR$^{-/-}$ carriers contained phosphorylated (i.e., activated) STAT1 (P-STAT1) upon challenge (Fig. 5 B). Accumulations of P-STAT1$^+$ cells were spatially associated with T cell clusters (Fig. 5 C), as revealed by computer-based cluster analysis (for details see Materials and methods). Within these areas, P-STAT1$^+$ cells were frequently in immediate contact with infiltrating T cells (Fig. 5 D). Co-immunostaining revealed that 94.2 ± 0.1% of P-STAT1$^+$ cells expressed the neuronal marker NeuN (mean ± SEM, $n = 3$ animals; Fig. 5 E). Moreover, 73 ± 6.7% of these P-STAT1$^+$ neurons expressed viral antigen (Fig. 5 E), as opposed to only 29 ± 6.1% rLCMV/INDG-infected neurons overall, suggesting an antigen-driven process. Besides STAT1, STAT3 can also signal downstream of the IFNGR (Ramana et al., 2002). However, only a minority of P-STAT3$^+$ cells colocalized with the neuronal marker NeuN (11.2 ± 7.2%), and P-STAT3$^+$ neurons were significantly less abundant (4.9 ± 1.7 cells/mm^2) than P-STAT1$^+$ neurons (30.4 ± 9.9 cells/mm^2, $P < 0.05$). These observations suggested a T cell–driven IFN-γ–STAT1 signaling pathway, which occurred preferentially in viral antigen-expressing neurons.

Inflammatory infiltrates in the viral déjà vu model are dominated by CD8$^+$ T cells (Merkler et al., 2006). Hence we set out to determine the role of CTL-derived IFN-γ in the disease process. After lethal irradiation, we reconstituted WT mice with a mixture of CD8$^{-/-}$ bone marrow (2/3 of the transferred cells) plus either WT or IFN-γ–deficient (GKO) bone marrow (1/3 of the transferred cells). In the resulting

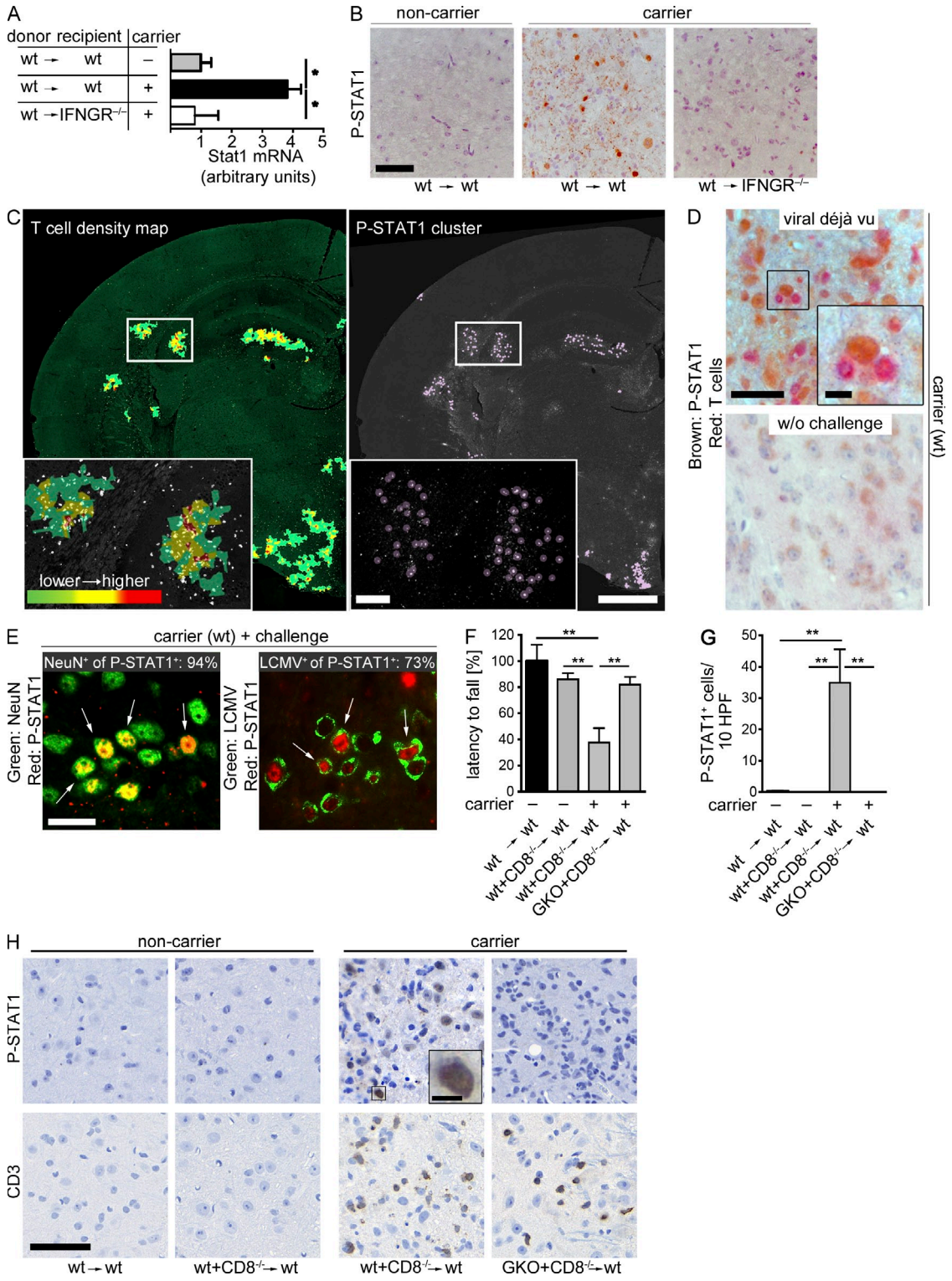

Figure 5. STAT1 up-regulation, phosphorylation, and nuclear translocation reflect the neuronal signature of IFN-γ signaling. (A–H) Viral déjà vu experiments were conducted with bone marrow chimeric mice of the indicated genotypes and carrier state. Carrier mice and noncarrier controls were challenged with LCMVwt (10^4 PFU) i.v. in adulthood. Experiments were analyzed on day 10 after challenge. (A) STAT1 mRNA levels were assessed by qPCR. Error bars indicate the mean + SEM of 4–6 mice. (B) Immunohistochemistry for phosphorylated STAT1 (P-STAT1) was performed on brain sections of WT→WT carriers, WT→IFNGR$^{-/-}$ carriers, and noncarrier controls. (C, left) T cell density map visualizes hot spots of inflammatory infiltrates. (C, right) P-STAT1$^+$ neurons (visualized as purple spheres) within the same section. (D) Juxtaposition of P-STAT1$^+$ (brown) cells and T cells (red) in challenged animals. (E, left) Colocalization of P-STAT1$^+$ (red) with neurons (NeuN, green). (E, right) Colocalization of P-STAT1$^+$ (red) with LCMV-NP (green). Arrows indicate

GKO^{+}CD8$^{-/-}$→WT chimeric mice, CD8^{+}T cells were IFN-γ–deficient, whereas the majority of all other hematopoietic cells as well as nonhematopoietic cells were IFN-γ–competent. In control WT^{+}CD8$^{-/-}$→WT mice, all cell populations contained a functional IFN-γ gene. When subjected to challenge, GKO^{+}CD8$^{-/-}$→WT chimeric mice, unlike WT+CD8$^{-/-}$→WT control mice, did not develop disease and did not show neuronal P-STAT1 expression (Fig. 5, F–H). This result demonstrates that CD8^{+} T cell–derived IFN-γ is essential for neuronal STAT1 signaling and viral déjà vu disease.

To address whether IFNGR expression by virus-infected neurons was necessary for viral déjà vu disease, we used mice with a conditional allele of the IFNGR (IFNGR$^{fl/fl}$). Neonatal inoculation of a recombinant rLCMV/INDG-expressing Cre recombinase (rLCMV-Cre) disrupted the IFNGR gene selectively in virus-infected cells (Fig. 6). To validate the experimental setting, we confirmed the cellular tropism and Cre recombinase activity of rLCMV-Cre in loxP-flanked RFP reporter mice (Luche et al., 2007). Co-immunostaining of LCMV-NP with the neuronal marker NeuN confirmed that rLCMV-Cre, like rLCMV/INDG (Merkler et al., 2006), persisted exclusively in neurons (Fig. 6 A). Moreover, 99.0 ± 0.6% of LCMV-NP^{+} neurons expressed RFP reporter, thus attesting to efficient LCMV-Cre–mediated recombination of loxP sites in vivo (Fig. 6 A). Indeed, WT but not IFNGR$^{fl/fl}$ carriers of rLCMV/IND-Cre developed viral déjà vu disease (Fig. 6 B) despite comparable CD8 T cell infiltrates in the CNS (Fig. 6, C,D, and G). Accordingly, the density of perisomatic boutons in rLCMVIND-Cre IFNGR$^{fl/fl}$ carriers remained normal (Fig. 6, E and G), and only few P-STAT1^{+} cells were detected in the brain (Fig. 6, F and G). In a complementary approach, we crossed IFNGR$^{fl/fl}$ animals with mice constitutively expressing the Cre recombinase under a neuron-specific Thy1 promoter (Thy1-cre x IFNGR$^{fl/fl}$; Dewachter et al., 2002), thereby disrupting IFNGR signaling selectively in neurons. Thy1-Cre x IFNGR$^{fl/fl}$ mice were resistant to viral déjà vu disease (Fig. 6 H). Both experimental settings supported the conclusion that IFNGR signaling in virus-infected neurons was essential for the disease process.

IFN-γ blockade prevents neuronal deafferentation and clinical disease upon challenge but does not prevent lethal CTL-mediated choriomeningitis

The above findings in mice suggested that the IFN-γ–STAT1 axis represented a conserved pathway to deafferentation, largely accounting for acute clinical disease upon CTL attack on neurons. Hence, we investigated whether this mechanistic knowledge could be translated into neuroprotective intervention. Carrier mice were given IFN-γ–blocking antibody or isotype control treatment (Abrams et al., 1992) on day 5 after challenge, thus avoiding interference with the induction, expansion, or maturation of the CTL response (Fig. 7). Indeed, IFN-γ blockade did not alter the magnitude of NP396-specific CTL responses in peripheral blood of carrier mice (not depicted), but it protected against clinical manifestations of viral déjà vu disease (Fig. 7 A). Histological analysis showed that IFN-γ blockade did not affect CTL invasion into the CNS either (Fig. 7, B, C, and F) but prevented CTL-mediated deafferentation (Fig. 7, D and F). In support of our previous conclusions that IFN-γ accounted for neuronal STAT1 signaling (Fig. 5), IFN-γ blockade prevented STAT1 phosphorylation in neurons of mice after challenge (Fig. 7, E and F). In situ detection of the administered antibody confirmed its penetration into the inflamed CNS parenchyma of carriers with viral déjà vu disease (Fig. 7 G). Importantly, however, IFN-γ blocking antibody failed to afford any protection in the classical model of LCMV-induced choriomeningitis, an unrelated model of CNS disease; IFN-γ-depleted (n = 4) and isotype antibody control-treated animals (n = 3) both developed terminal choriomeningitis within 6–7 d after i.c. infection with LCMVwt (unpublished data). In this archetypal disease model, the virus spreads inside the meninges, ependyma, choroid plexus, and astrocytes forming the blood-brain barrier (but not in neurons as in the viral déjà vu setting), which then become targets of CTL attack (Cole et al., 1972). This confirmed that IFN-γ–blocking antibody administration on day 5 after challenge did not impair the pathogenic capacity of the ensuing CTL response altogether and, thus, that the IFN-γ–STAT1 axis was of selective importance for CTL attack on neurons but not for damage to other cell types of the CNS such as meninges and choroid plexus.

Neuronal deafferentation and IFN-γ signature are found in human RE

To investigate whether the neuronal IFN-γ signature observed in the viral déjà vu model represented a common trait of CTL-mediated neurological disease, we analyzed brain biopsies of human patients suffering from RE. At the histopathological level, RE is dominated by putatively antigen-specific CTL infiltrates in close association with CNS neurons (Schwab et al., 2009). Five out of six Rasmussen specimens displayed P-STAT1^{+} cells. CTLs were more diffusely disseminated, whereas P-STAT1^{+} cells were often clustered at various sites in the cerebral cortex and showed cellular colocalization

double-positive cells. 94% of P-STAT1^{+} cells were NeuN^{+} (616 neurons analyzed from three mice). 73% of P-STAT1^{+} neurons were LCMV-NP^{+} (105 neurons analyzed from three mice). (F–H) Lethally irradiated WT mice, carriers or noncarriers, were reconstituted with either CD8$^{-/-}$ plus IFN-γ–deficient (GKO) or CD8$^{-/-}$ plus WT bone marrow at a 3:1 ratio (CD8$^{-/-}$: GKO or CD8$^{-/-}$: WT, respectively). Shown are rotarod performance (F), density of P-STAT1^{+} cells (G), and representative histological brain sections from the respective animals (H). Symbols represent the mean + SEM . Bars: (B) 70 µm; (C) 300 µm; (C, inset) 100 µm; (D and H) 50 µm; (D, inset) 10 µm; (E) 20 µm; (H, inset) 12.5 µm. HPF: high power field. A–D show representative data from one out of two similar experiments with 4–6 animals per group. E shows representative data from 3 animals per group and staining. Error bars in F and G represent the mean + SEM of 7–11 animals from one experiment. *, P < 0.05; **, P < 0.01.

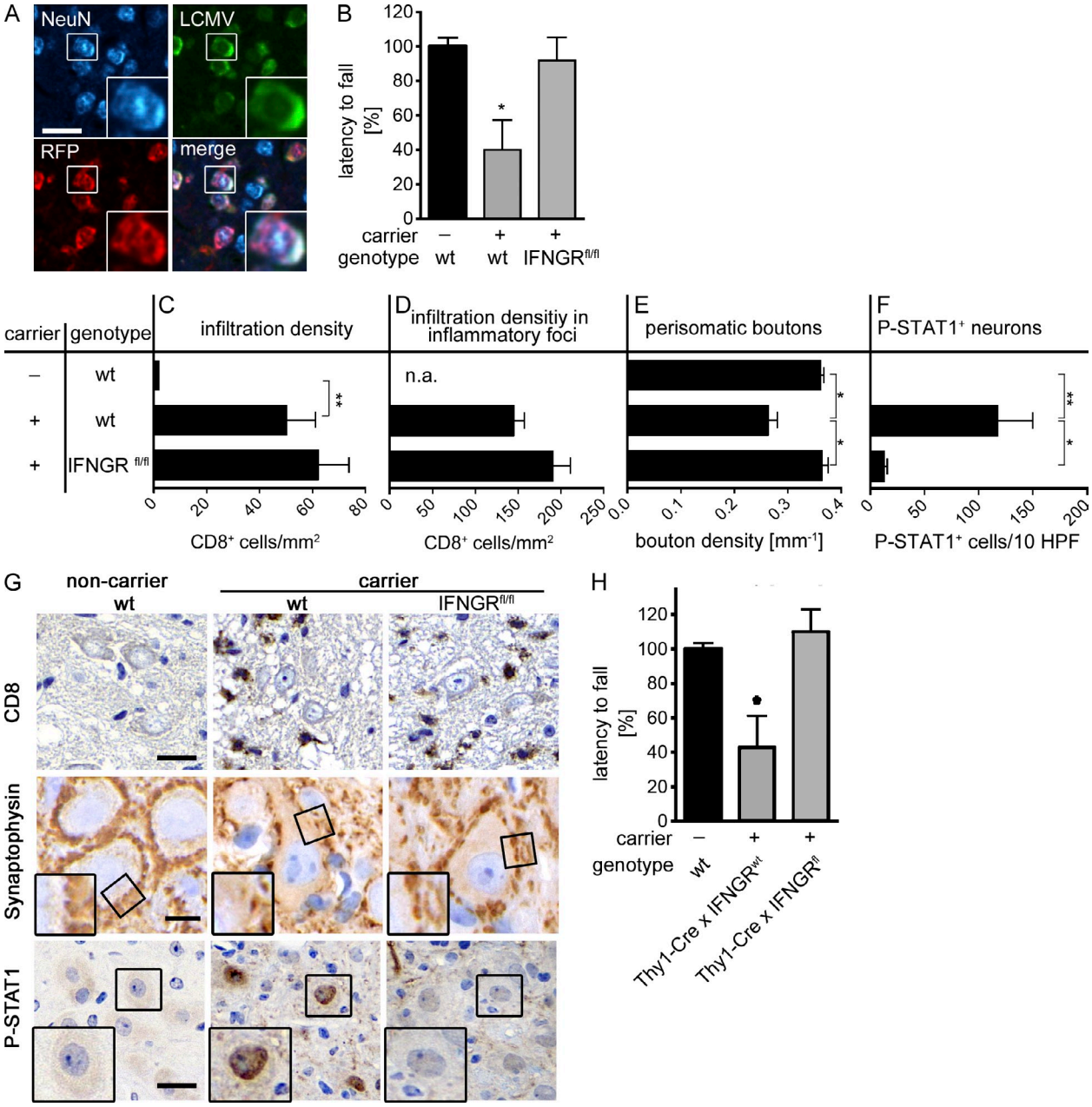

Figure 6. Selective disruption of IFN-γ signaling in virus-infected neurons protects from clinical disease and neuronal deafferentation upon challenge. (A) Reporter mice expressing tandem RFP after Cre-mediated recombination were neonatally infected with Cre-expressing rLCMV/INDG (rLCMV-Cre). Representative images of adult rLCMV-Cre carrier reporter mice show virus antigen (LCMV-NP, green) in neurons (NeuN, cyan) coexpressing RFP (red), thus confirming efficient virus-induced Cre-mediated recombination in infected neurons (at least 275 cortical neurons were evaluated from 3 mice each). (B–G) Adult WT noncarrier controls and rLCMV-Cre carrier mice with a conditional IFNGR allele ($IFNGR^{fl/fl}$) or WT mice, respectively, were challenged with LCMVwt (10^4 PFU) i.v. Rotarod performance (B), brain-infiltrating CTL numbers (C and D), perisomatic bouton density in the DCN (E), and the density of cerebellar P-STAT1+ neurons (F) were analyzed at the peak of disease (day 10 after challenge). (G) Representative images of CTL infiltrates (top row), synaptophysin (middle row), and P-STAT1+ cells (bottom row) of the indicated groups. (H) Mice with disrupted IFNGR expression in neurons (Thy1-Cre x $IFNGR^{fl/fl}$) mice were infected and challenged as in Fig. 2 A. Rotarod performance at the peak of disease (day 10 after challenge) is shown. Error bars represent the mean + SEM. HPF: high power field. Bars: (A; G, CD8 and P-STAT1) 25 µm; (G, synaptophysin) 10 µm. Data are from 9–11 animals per group for B, 3 animals for A, 4–5 animals for C–G, and 5–11 animals for H. Representative data from one out of two similar experiments are shown. *, $P < 0.05$; **, $P < 0.01$.

with the neuronal marker NeuN (Fig. 8 A). Interestingly, P-STAT1+ neurons were often in close contact with CD8+ T cells (Fig. 8 B). CTL infiltration density varied considerably between different RE specimens, as expected for different disease stages (Pardo et al., 2004), and correlated positively with the density of P-STAT1+ neurons ($P < 0.05$, $r^2 = 0.76$,

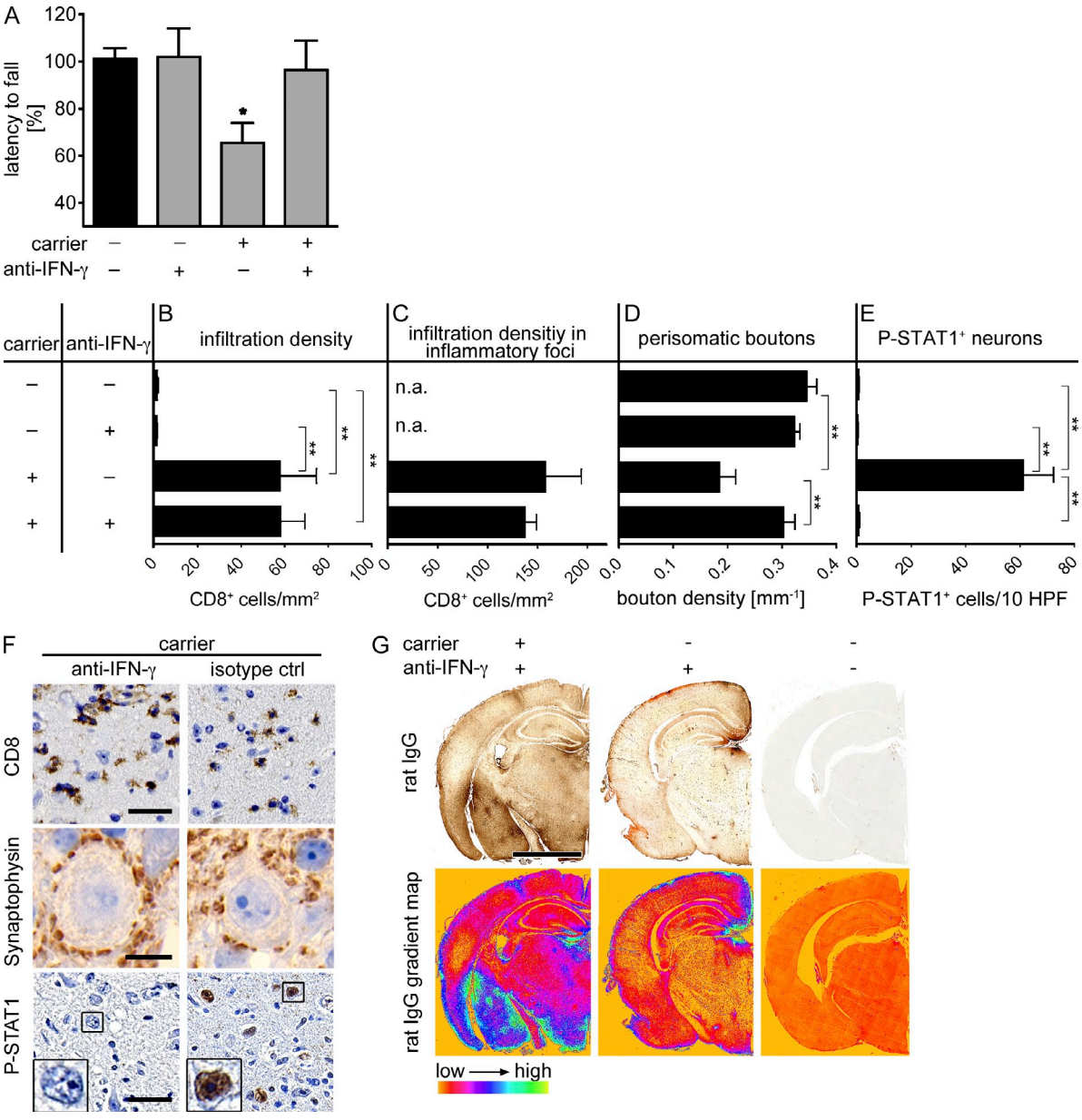

Figure 7. IFN-γ blockade prevents neuronal deafferentation and clinical disease upon challenge. (A–E) Virus carriers and noncarrier controls were challenged with LCMV (10^4 PFU) i.v. 5 d later, IFN-γ–blocking antibody (XMG1.2, indicated as +) or isotype control antibody (indicated as –) was administered i.p. to carrier mice and noncarrier controls as indicated in the chart. Rotarod performance (A), brain-infiltrating CTL numbers (B, C, and F), perisomatic bouton density in the DCN (D and F), the density of cerebellar P-STAT1⁺ neurons (E and F), and in situ detection of anti–IFN-γ–blocking antibody (G) were analyzed at the peak of disease (day 10 after challenge). (F) Representative images of CTL infiltrates (top row), synaptophysin (middle row), and P-STAT1⁺ cells (bottom row) from the indicated groups are shown. (G) Representative images of in situ detected anti–IFN-γ–blocking antibody (brown reaction in top panel) and corresponding gradient map (bottom panel) of the indicated groups are shown. Error bars represent the mean + SEM. HPF: high power field. Bars: (F, CD8 and P-STAT1) 50 µm; (F, synaptophysin) 10 µm; (G) 2 mm. Data are from 6–9 animals per group for A–C, E, and G, and 3–6 animals per group for D. F shows representative images from the animals evaluated in B–E. Representative data from one out of two similar experiments are shown. *, $P < 0.05$; **, $P < 0.01$; n.a., not applicable.

n = 6 patients; Fig. 8 C). To investigate whether neuronal P-STAT1 expression was spatially associated with CTL infiltration, we generated a CTL density map from a representative RE biopsy specimen (Fig. 8 D). Computational analysis confirmed that in analogy to the viral déjà vu setting (Fig. 5 C), 70% of P-STAT1 neurons were situated within CTL "hot-spots" which represented only a minute proportion (0.12%) of the total biopsy area. In further analogy to the viral déjà vu model, the density of perisomatic synapses on P-STAT1–positive neurons was significantly reduced as compared with those on P-STAT1–negative neurons in close vicinity (Fig. 8 E).

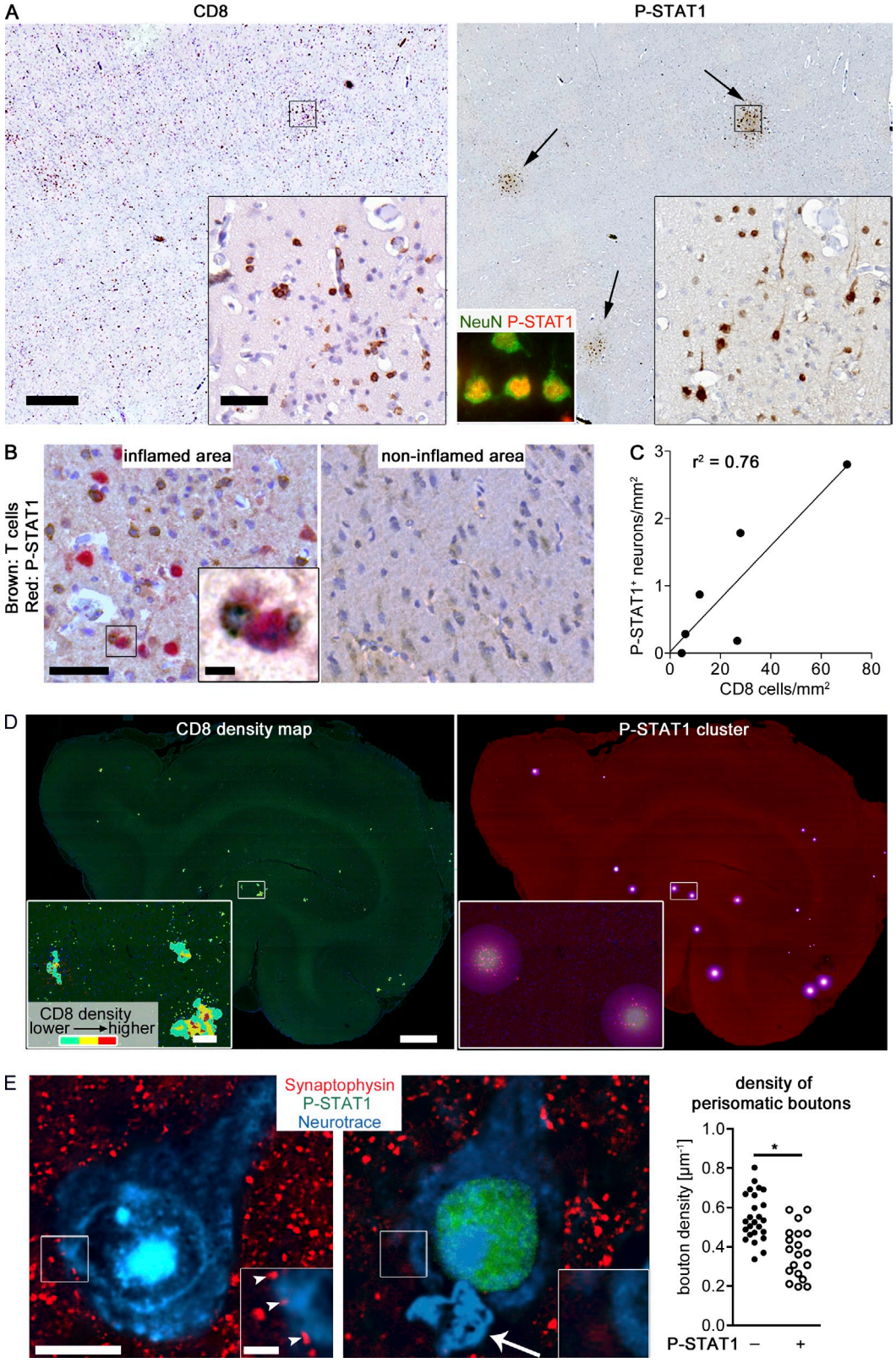

Figure 8. Neuronal STAT1 phosphorylation and reduced synaptic boutons in CD8⁺ T cell clusters of human RE. (A–E) Brain specimen from human RE. (A) Representative image of RE biopsy stained for CD8 (left) or P-STAT1 (right) on adjacent brain sections. Fluorescence inset shows cellular overlap of P-STAT1 (red) with neuronal marker NeuN (green). Arrows point to clusters of P-STAT1⁺ cortical neurons. (B) Co-immunostaining for CD8⁺ T cell infiltrates (brown) and P-STAT1 neurons (red) in inflamed and noninflamed brain area is shown. (C) Correlation between P-STAT1⁺ neurons and CD8⁺ T cell

DISCUSSION

The present study establishes deafferentation as an early morphological consequence of CTL attack on neurons, both in mice and in humans, and identifies IFN-γ as the central molecular mediator in vivo. Together with our proof-of-principle for antibody blockade in mice, these findings delineate a direct path to clinical translation. A humanized IFN-γ blocking antibody has previously demonstrated safety and efficacy in clinical trials for Crohn's disease (Hommes et al., 2006; Reinisch et al., 2010), facilitating its exploratory administration for the treatment of RE and related immunological CNS disorders. Further, the intracellular signaling pathways downstream of the IFNGR are well characterized, comprising druggable targets (Platanias, 2005). Neuronal deafferentation apparently results from a fairly pinpointed attack by CTLs engaging antigen-expressing target neurons. Hence, IFN-γ blocking agents need to act at the CTL–neuron synapse and have to pass the blood-brain barrier. Small molecule inhibitors offer advantages in this regard, but antibodies can also pass at sites of inflammation, and thus may be selectively delivered to the appropriate place. Increased permeability of the blood brain barrier in typically young RE patients may further facilitate this process.

Our findings match previous in vitro observations that IFNGR-STAT1 signaling can cause dendritic retractions and inhibit synapse formation by cultured neurons (Kim et al., 2002). Several mechanisms may account for this. First, IFN-γ can reduce cytoplasmic ATP levels (Mizuno et al., 2008), which may induce bioenergetic failure and ionic imbalances. Indeed, reduced ATP production is characteristic of neurons inside MS lesions (Dutta et al., 2006; Mahad et al., 2009; Campbell et al., 2011). Second, the IFNGR may form a complex with the AMPA receptor subunit GluR1 in neurons, leading to increased excitability and vulnerability to glutamate excitotoxicity (Mizuno et al., 2008). It thus seems plausible that CTL-derived IFN-γ sensitizes inflamed brain regions to epileptic seizures, which represents the earliest and most prominent manifestation of RE (Rasmussen et al., 1958; Bien et al., 2005). Of note, our present findings offer a potential explanation for the disease-enhancing effects of IFN-γ in an exploratory trial for MS (Panitch et al., 1987), a disease with prominent dendritic pathology. With this postulate, we do not, however, mean to exclude the possibility that inhibitory effects of IFN-γ on remyelination (Lin et al., 2006) and/or its immunostimulatory activity may also contribute to the adverse effects in MS.

Our observations may seem contradictory to earlier results emphasizing perforin- and Fas-dependent cytolysis of neurons (Medana et al., 2000; Meuth et al., 2009; Sobottka et al., 2009). Yet the viral déjà vu model is deliberately focused on the acute phase of CTL-mediated disease, which is of primary therapeutic relevance. Indeed, consequences of perforin- and/or Fas-mediated killing are likely more relevant in advanced stages of inflammatory CNS disease. Neuronal loss is a dominant feature in chronic but not acute stages of RE (Bien et al., 2002; Pardo et al., 2004) and was observed only late after challenge (Fig. 1). Deafferentation and cytolysis might thus represent sequential steps. Electrical silencing is known to render cultured neurons susceptible to CTL lysis (Neumann et al., 1995), but mechanisms of neuron silencing in vivo and its relevance have remained unclear. Our observations offer a unifying explanation: IFN-γ signaling in neurons may cause deafferentation, thus reducing synaptic drive below a critical threshold (Neumann et al., 1995). As a consequence and also driven by IFN-γ directly (Neumann et al., 1997), MHC-I expression may increase (Scheikl et al., 2012) and ultimately render neurons susceptible to perforin- or Fas-mediated cytolysis. Consistent with this concept, IFN-γ expression was found to be elevated in early RE, whereas expression of FAS ligand correlated with tissue destruction in later disease stages (Owens et al., 2013). Demyelination, as found in MS, may further facilitate lytic CTL attack by exposing axons (Deb et al., 2009). Analogously, in vitro culture conditions may have facilitated neuronal cytolysis by $CD8^+$ T cells (Medana et al., 2000; Meuth et al., 2009; Sobottka et al., 2009), stressing the importance of a direct in vivo investigation of effector mechanisms as performed here.

Efficient CTL killing of virus-infected neurons would be to the obvious detriment of the host, and thus may have been selected against during evolution (Joly and Oldstone, 1992). Considering the severe consequences described here, the evolutionary conservation of neuronal IFN-γ sensing may come as a surprise. We propose that IFN-γ sensitivity was retained to allow for noncytolytic viral clearance from neurons, a known key function of IFN-γ in the CNS (Binder and Griffin, 2001). It comes at the expense of isolating the respective neurons from their synaptic networks, which likely is reversible (Zhang et al., 2005; Nikić et al., 2011). Hence, transient isolation of neurons from the circuits might represent an "affordable" strategy to clear viruses from infected neurons while avoiding the irreversible loss of these postmitotic cells. Conversely, therapeutic IFN-γ blockade could influence viral clearance (Binder and Griffin, 2001; Burdeinick-Kerr and Griffin, 2005). Collectively, the identification of CTL-driven neuronal deafferentation by the IFN-γ signaling pathway recasts our concept of "immune privilege" and host–pathogen

infiltration density. Symbols represent individual RE patients ($n = 6$). (D, left) A CD8 density map visualizes CTL hot spots in a temporal lobe. (D, right) P-STAT1$^+$ neurons (visualized as pink spheres) within the same biopsy. (E, left) Coimmunostaining of synaptophysin (red), P-STAT1 (green), and Neurotrace (cyan). Synaptophysin$^+$ (red) perisomatic bouton density (arrowheads) on P-STAT1$^+$ (green) is reduced as compared with P-STAT1$^-$ neurons. Arrow points to a T cell found in contact with a P-STAT1$^+$ neuron. (E, right) Quantification of perisomatic bouton density. Symbols represent individual neurons. Bars: (A, overview and D, inset) 500 µm; (B, overview and A, inset) 50 µm; (B, inset and E, overview) 10 µm; (D, overview) 2 mm; (E, inset) 2 µm. Brain biopsies of 6 different RE patients were analyzed. *, $P < 0.05$.

interactions in the CNS, with potentially wide-ranging implications for neuroprotective strategies in viral and autoimmune CNS disease.

MATERIALS AND METHODS

Mice. Mice in this study included C57BL/6 WT mice, mice deficient for perforin (PKO; Kägi et al., 1994), TNF receptor 1 and 2 (TNFR1/2$^{-/-}$; Peschon et al., 1998), Fas (FAS$^{-/-}$; Adachi et al., 1995), or IFNGR$^{-/-}$ (Huang et al., 1993), transgenic mice overexpressing the MHC class I molecule H-2D^b in neurons (NSE-D^b; Rall et al., 1995; provided by D.B. McGavern and M.B.A. Oldstone, the Scripps Research Institute, La Jolla, CA), RAG2-deficient (Shinkai et al., 1992) P14 TCR-transgenic mice (P14xRAG) expressing a TCR specific for amino acids 33–41 of the LCMV glycoprotein in the context of H-2D^b (Pircher et al., 1989), *Thy1*-YFP-H mice, which express YFP in a subset of neurons (Feng et al., 2000), and Thy1-cre mice expressing the cre recombinase in neurons of the CNS (Dewachter et al., 2002; provided by M. Schwab, Brain Research Institute, University and ETH Zurich, Switzerland). Mice expressing the conditional IFNGR (IFNGR$^{fl/fl}$) were generated by gene targeting in murine IDG32 F1 cells (provided by R. Kuhn, Helmholz Centre Munich, Germany) of the C57BL/6 × 129 strain and were backcrossed on C57BL/6 for eight generations. In the conditional allele, exons 4–6 are flanked by loxP sites. Deletion of these exons leads to inactivation of IFN-γ signaling. Cells with two floxed alleles signal comparably to controls. Their full characterization will be published elsewhere. NSE-D^b x IFNGR$^{-/-}$ and Thy1-Cre x IFNGR$^{fl/fl}$ were generated by intercrossing. All mice were generated on C57BL/6 or backcrossed on C57BL/6 background (eight or more generations). Animal experiments were performed at the Universities of Geneva and Zurich with authorization by the responsible Cantonal authority and in accordance with the Swiss law for animal protection, and at the University of Göttingen with authorization by the Bezirksregierung Braunschweig in accordance with the German law for animal protection.

Human tissue. Brain biopsies (n = 6) from patients with RE were obtained from the collection of the Department of Neuropathology at the Universitätsklinikum Erlangen. Patients 1–6 were 15, 8, 9, 3, 42, or 7 yr old with disease duration between 1 and 9 yr at the time of surgery. Their use for scientific purposes was in accordance with institutional ethical guidelines and was approved by the ethics committee of the University of Göttingen (Germany).

Virus infection, titrations, and inoculations, and detection of viral RNA. A TaqMan RT-PCR protocol targeting the LCMV-NP gene (Pinschewer et al., 2010a) was used to quantify rLCMV/INDG S segment copies in the brain of infected mice. Arbitrary viral RNA units were determined in a multiplex assay with a commercial kit for detection of the housekeeping gene GAPDH serving as internal reference (Applied Biosystems). Viruses were produced, titrated, and administered to mice as previously reported (Merkler et al., 2006). For i.c. infection with LCMVwt the Armstrong strain was used at a dose of 10^3 PFU. Cre recombinase–expressing rLCMV-Cre was generated according to established procedures (Emonet et al., 2009).

Viral déjà vu setup, bone marrow reconstitution, and in vivo blockade of IFN-γ. Neonatal C57BL/6 (WT), IFNGR$^{-/-}$, TNFR1/2$^{-/-}$, FAS$^{-/-}$, and PKO mice were infected with rLCMV/INDG i.c. to establish a viral carrier status in neurons as described previously (Merkler et al., 2006). Control groups of C57BL/6 mice were left uninfected at birth. At the age of 5–6 wk, all mice were lethally irradiated. IFNGR$^{-/-}$, TNFR1/2$^{-/-}$, or FAS$^{-/-}$ mice were reconstituted with C57BL/6 (WT) bone marrow and splenocytes. To have standardized conditions when assessing the role of perforin in viral déjà vu disease, PKO carrier mice were irradiated analogously to the other groups and were reconstituted with PKO bone marrow cells. As a complicating factor for this analysis, perforin-deficient (PKO) mice cannot control LCMVwt and develop severe wasting disease unrelated to the viral déjà vu pathology (Kägi et al., 1994). To reconstitute LCMVwt control in PKO mice, we adoptively transferred 10^4 perforin-competent P14 T cell receptor-transgenic CD8$^+$ T cell–containing splenocytes (P14xRAG) i.v. on day −1 of challenge. These RAG2-deficient and hence monoclonal cells respond to an epitope derived from the LCMVwt glycoprotein, which is only expressed by the LCMVwt challenge but not by rLCMV/INDG persisting in virus carrier neurons. Hence, perforin-competent P14xRAG cells controlled peripheral challenge with LCMVwt in PKO mice but they could not attack CNS neurons persistently infected with rLCMV/INDG. 4–8 wk after bone marrow reconstitution, the animals were challenged, i.e., 10^4 PFU LCMVwt was administered i.v. to trigger a vigorous NP396-specific CTL response. For in vivo blockade of IFN-γ, mice were given a single dose of 2 mg rat anti–IFN-γ monoclonal antibody (clone: XMG1.2, BioXcell) or isotype control antibody (anti-HRPN; BioXcell) by i.p. administration on day 5 after challenge or i.c. (choriomeningitis model) infection.

Rotarod. The ability of motor coordination and balance of mice was monitored with the rotarod test. In this assay, a mouse is placed on a rotating rod that gradually increases its speed of rotation. Thus, the locomotor performance as measured by the time the animal stays on the rotating rod reflects the maximum rotation speed of the rod up to which the animal can stay in balance. Specifically, mice were placed on a rotating rod (Rotarod 7650; Ugo Basile Biological Research Apparatus) constantly accelerating from 4 to 40 rounds per minute for a maximum of 180 s. Animals were habituated and trained to the rotarod daily from day −3 to day 0, as well on days 3, 5, and 7–10. Endurance time was monitored, and the two best runs out of three at each time point were averaged for analysis. Values are displayed as percentage of healthy noncarrier controls on day 10.

Brain-extracted lymphocytes and flow cytometry. Lymphocytes were extracted from brains as described previously (Merkler et al., 2006). Epitope-specific IFN-γ – and TNF-producing and MHC class I tetramer–binding CD8$^+$ T cells were detected by flow cytometric analysis, as described previously (Probst et al., 2003). Allophycocyanin-conjugated anti–IFN-γ, FITC-conjugated anti-TNF, PE-conjugated anti-CD8β and anti-CD8α, and peridinin-chlorophyll protein–conjugated anti-B220 antibodies were purchased from BD. The frequency of IFN-γ$^+$CD8$^+$ or tetramer$^+$CD8$^+$ cells was calculated as a percentage of CD8$^+$B220$^-$ lymphocytes.

Histopathology. CNS tissue was either fixed with 4% paraformaldehyde or in HOPE fixative (DCS Innovative; Olert et al., 2001) and was embedded in paraffin as described previously (Bergthaler et al., 2007). For light microscopy, endogenous peroxidases (PBS/3% H_2O_2) were neutralized and unspecific binding blocked (PBS/10% FCS). PFA-fixed sections were stained with primary antibodies: rat anti–human CD3 (cross-reactive with murine T cells; Serotec), mouse anti-neuronal nuclei NeuN (EMD Millipore), rabbit anti–Iba-1 (microglia/macrophages; Wako Chemicals USA), rat anti-LCMV nucleoprotein sera (generated by prime-boost immunization against purified LCMV-NP), rabbit anti–phospho-STAT1 (detecting only phosphorylated STAT1 at position Tyrosine 701; Cell Signaling Technology), mouse anti–rat synaptophysin (cross-reactive with mouse; clone SY38c; Dako), and mouse anti–human CD8 (clone C8/114B; Dako). Hope-fixed sections were stained using rat anti–mouse CD8 antibody YTS169 and rat anti-LCMV nucleoprotein antibody (VL-4; Battegay et al., 1991). Rat anti–IFN-γ monoclonal antibody was detected in situ on hope-fixed sections using biotinylated anti–rat antibody. Bound primary antibodies were visualized either by an avidin-biotin technique with 3,3′-diaminobenzidine or alkaline phosphatase/anti–alkaline phosphatase as chromogens (haemalaun counterstaining of nuclei) for light microscopy or with the appropriate species-specific Cy2-, Cy3-, or Cy5-conjugated secondary antibodies (all from Jackson ImmunoResearch Laboratories, Inc.) with DAPI (Sigma-Aldrich) nuclei or Neurotrace (Invitrogen) nuclei/Nissl counterstaining for fluorescence microscopy.

Confocal microscopy. We obtained confocal images of fixed spinal cord sections of *Thy1*-YFP-H mice on an FV1000 confocal system mounted on an upright BX61 microscope (Olympus) equipped with 20×/0.85 and 60×/1.42 oil immersion objectives. We recorded stacks of 12-bit images that

were subsequently processed using the free-ware Fiji/ImageJ (National Institutes of Health) to generate maximum intensity projections. To obtain final visualizations, these maximum intensity projections were further processed in Photoshop (Adobe) using gamma adjustments to enhance visibility of intermediate gray values and despeckle filtering to suppress detector noise, where necessary.

Quantification of inflammatory infiltrates, P-STAT1$^+$ neurons, and densitometry. For each animal, a total brain area of ≥15 × 10^6 μm^2 was analyzed at 200× magnification to calculate the mean number of CD8$^+$ cells/mm^2. Inflammatory foci in the DCN were defined as areas with >10 CD8$^+$ T cells per high-power visual field. Mean T cell densities within inflammatory foci were also assessed. The number of perisomatic synatophysin-positive boutons and the length of the somatic circumference of DCN neurons were quantified using analySIS software (Olympus) on either single-stained (synaptophysin) or triple-stained sections (synaptophysin, CD3 and LCMV; Fig. 2 B) at 1,000× magnification. The density of boutons per micrometer of neuronal circumference was calculated. Densitometric measurements of MAP-2$^+$ ventromedial dendrites in the spinal cord were performed using analySIS software. Human biopsies were scanned using the mirax slide scanner (Carl Zeiss) at 200× magnification. P-STAT1–positive neurons were manually counted in the cerebral cortex within an area of at least 17 × 10^6 μm^2.

To quantify neuronal cell densities in the CNS, we applied a custom-made script, which was based on Cognition Network Language (Definiens Cognition Network Technology; Definiens Developer XD software) and resembled a previously described one (Manrique-Hoyos et al., 2012). In brief, paraffin-embedded brain sections were stained by immunohistochemistry using NeuN (antibody specifications and staining procedure are described in the Histopathology section). Stained sections were scanned using the mirax slide scanner at 200×. The areas of interest in the hippocampus (dentate gyrus), cerebral cortex, hypothalamic nucleus, brain stem, and ventral horn of cervical and thoracic spinal cord were identified using a mouse brain atlas. Region of interest were drawn manually on the scanned images. NeuN-positive structures within the area of interest were first detected based on their color spectrum. After detailed segmentation, nucleus and cytoplasm were discriminated. An image object was classified as a neuron if 0–1 nucleus was detected within a detected cytoplasm. If more than one nucleus was detected within a detected cytoplasm, nuclei served as seed points growing into the surrounding cytoplasm. Image objects were then split at the site where growing borders converged. Within each area of interest, the total number of neurons was enumerated and the density of NeuN-positive cells was calculated and expressed as cells/mm^2.

Generation of T cell density map. Brain sections were co-immunostained for T cells, P-STAT1, and DAPI (antibody specifications and staining procedure are described in the Histopathology section) and registered using the slide scanner Pannoramic 250 Flash (3DHistech) at 200×, generating a digitalized 8-bit color RGB image (with 256 levels of brightness) from the whole specimen. To analyze the distribution patterns of T cells in the human RE biopsy and viral déjà vu, we developed an image analysis ruleset based on the Definiens Cognition Network Language; in brief, the tissue was detected and separated from background by its higher brightness (brightness value > 20 in all image layers). Detected tissue was then segmented using a multi-threshold segmentation calculating the threshold dividing the selected set of pixels into two subsets, so that heterogeneity is increased to a maximum. This segmentation was performed on the red as well as on the green image channel. P-STAT1 and T cell signals cells were then detected by their brightness values in the corresponding RGB channels (for P-STAT1, >85; for T cells, >70). Autofluorescence was detected based on the ratio of spatially overlapping red/green signal (ratio between 0.4 and 2) and excluded from further analysis.

Next, an additional image layer was created containing the pixel distances between neighboring T cells as gray values using the distance map algorithm. For this purpose, the borders of image objects classified as T cells were grown along a distance gradient until establishing contact with the growing signal of neighboring T cell or reaching a maximal distance of 30 pixels. The mean distance values at the border of two neighboring T cells was calculated and T cells were classified as follows: class I, distance value of <20 (human) or <25 (mouse) pixels (light green); class II, distance value between 10 and 15 (human) or 15 and 20 (mice) pixels (yellow); class III, distance values <10 (human) or <15 (mouse) pixels (red). T cells with distance value > 25 were considered as having no close neighbors. CD8 cluster were defined as groups of more than five T cells belonging to either of the aforementioned class I–III. Furthermore, T cells situated within the perivascular, ependymal, or meningeal space were excluded from further analysis. The detected T clusters were then superimposed onto the stained tissue to correlate the spatial distribution with detected P-STAT1 signals.

Statistical analysis. Analyses were performed with SPSS software (version 12.0) and GraphPad Prism software (version 5.0). To assess significant differences between single measurements of two groups, two-tailed Student's *t* tests were used, whereas differences between single measurements of more than two groups were assessed by one-way ANOVA followed by multiple *t* tests with Bonferroni's adjustment for multiple comparisons if the F test of ANOVA indicated statistically significant differences. Two-way ANOVA was performed to test for differences between multiple measurements of two or more groups, again followed by multiple *t* tests with Bonferroni's adjustment for multiple comparisons if the F test of ANOVA indicated statistically significant differences. For comparisons to reference values or to values of a control group, one-way ANOVA followed by Dunnett's *t* tests were performed. Viral RNA loads were log-transformed for statistical analysis. Reduction in motor performance was tested in comparison to values before disease onset (day 0), which were set to 100%. A p-value <0.05 was considered significant, and p-values <0.01 were considered highly significant, whereas p-values >0.05 were considered statistically not significant.

We would like to thank L. Terry for critically reading the manuscript, C.-A. Siegrist and P.-H. Lambert for discussions, C. Schrick and Edit Horvath for technical support, D.B. McGavern and M.B.A. Oldstone for providing NSE-D^b transgenic mice, and M. Schwab for providing Thy1-cre mice. Ralf Kuhn (Helmholz centre Munich) provided the IDG32F1 ES cells.

D. Merkler and D.D. Pinschewer hold stipendiary professorships of the Swiss National Science Foundation (No. PP00P3_128372 to D. Merkler and No. PP00A-114913 to D.D Pinschewer.) and both are supported by the Klaus-Tschira Stiftung GmbH. T. Misgeld was supported by the Deutsche Forschungsgemeinschaft (DFG, SFB 596; and Center for Integrated Protein Science Munich, EXC 114 CIPSM), and by the German Federal Ministry of Research and Education ("Bundesministerium für Bildung und Forschung", BMBF) in the frame of ERA-Nets "ipsoALS" and "2photon imaging". M. Kerschensteiner was supported by grants from the DFG (Emmy-Noether Program, SFB 571 and Transregio 128) and the BMBF (Competence Network Multiple Sclerosis) and the Verein "Therapieforschung für MS-Kranke e.V." T. Misgeld and M. Kerschensteiner received support from the Munich Cluster for Systems Neurology (EXC 1010 SyNergy). D. Merkler and M. Kerschensteiner were further supported by a grant from the Gemeinnützige Hertie Stiftung. A. Bergthaler was a European Molecular Biology Organization long-term fellow and was supported by postdoctoral scholarships of the Roche Research Foundation and by the Schweizerische Stiftung für Medizinisch-Biologische Stipendien foundation (SSMBS) of the Swiss National Science Foundation (SNF). The generation of the conditional IFNGR2 mouse mutant by A. Fleige was supported by DFG (SFB 621 to W. Muller), and the primary characterization was supported by a BBSRC PhD stipend to R. Forman.

The authors have no conflicting financial interests.

Submitted: 22 September 2012
Accepted: 7 August 2013

REFERENCES

Abrams, J.S., M.G. Roncarolo, H. Yssel, U. Andersson, G.J. Gleich, and J.E. Silver. 1992. Strategies of anti-cytokine monoclonal antibody development: immunoassay of IL-10 and IL-5 in clinical samples. *Immunol. Rev.* 127:5–24. http://dx.doi.org/10.1111/j.1600-065X.1992.tb01406.x

Adachi, M., S. Suematsu, T. Kondo, J. Ogasawara, T. Tanaka, N. Yoshida, and S. Nagata. 1995. Targeted mutation in the Fas gene causes hyperplasia in

peripheral lymphoid organs and liver. *Nat. Genet.* 11:294–300. http://dx.doi.org/10.1038/ng1195-294

Albert, M.L., and R.B. Darnell. 2004. Paraneoplastic neurological degenerations: keys to tumour immunity. *Nat. Rev. Cancer.* 4:36–44. http://dx.doi.org/10.1038/nrc1255

Battegay, M., S. Cooper, A. Althage, J. Bänziger, H. Hengartner, and R.M. Zinkernagel. 1991. Quantification of lymphocytic choriomeningitis virus with an immunological focus assay in 24- or 96-well plates. *J. Virol. Methods.* 33:191–198. http://dx.doi.org/10.1016/0166-0934(91)90018-U

Bergthaler, A., D. Merkler, E. Horvath, L. Bestmann, and D.D. Pinschewer. 2007. Contributions of the lymphocytic choriomeningitis virus glycoprotein and polymerase to strain-specific differences in murine liver pathogenicity. *J. Gen. Virol.* 88:592–603. http://dx.doi.org/10.1099/vir.0.82428-0

Bien, C.G., H. Urbach, M. Deckert, J. Schramm, O.D. Wiestler, H. Lassmann, and C.E. Elger. 2002. Diagnosis and staging of Rasmussen's encephalitis by serial MRI and histopathology. *Neurology.* 58:250–257. http://dx.doi.org/10.1212/WNL.58.2.250

Bien, C.G., T. Granata, C. Antozzi, J.H. Cross, O. Dulac, M. Kurthen, H. Lassmann, R. Mantegazza, J.G. Villemure, R. Spreafico, and C.E. Elger. 2005. Pathogenesis, diagnosis and treatment of Rasmussen encephalitis: a European consensus statement. *Brain.* 128:454–471. http://dx.doi.org/10.1093/brain/awh415

Binder, G.K., and D.E. Griffin. 2001. Interferon-gamma-mediated site-specific clearance of alphavirus from CNS neurons. *Science.* 293:303–306. http://dx.doi.org/10.1126/science.1059742

Brown, S.M., J.H. Subak-Sharpe, K.G. Warren, Z. Wroblewska, and H. Koprowski. 1979. Detection by complementation of defective or uninducible (herpes simplex type 1) virus genomes latent in human ganglia. *Proc. Natl. Acad. Sci. USA.* 76:2364–2368. http://dx.doi.org/10.1073/pnas.76.5.2364

Burdeinick-Kerr, R., and D.E. Griffin. 2005. Gamma interferon-dependent, noncytolytic clearance of sindbis virus infection from neurons in vitro. *J. Virol.* 79:5374–5385. http://dx.doi.org/10.1128/JVI.79.9.5374-5385.2005

Campbell, G.R., I. Ziabreva, A.K. Reeve, K.J. Krishnan, R. Reynolds, O. Howell, H. Lassmann, D.M. Turnbull, and D.J. Mahad. 2011. Mitochondrial DNA deletions and neurodegeneration in multiple sclerosis. *Ann. Neurol.* 69:481–492. http://dx.doi.org/10.1002/ana.22109

Chevalier, G., E. Suberbielle, C. Monnet, V. Duplan, G. Martin-Blondel, F. Farrugia, G. Le Masson, R. Liblau, and D. Gonzalez-Dunia. 2011. Neurons are MHC class I-dependent targets for CD8 T cells upon neurotropic viral infection. *PLoS Pathog.* 7:e1002393. http://dx.doi.org/10.1371/journal.ppat.1002393

Cole, G.A., N. Nathanson, and R.A. Prendergast. 1972. Requirement for theta-bearing cells in lymphocytic choriomeningitis virus-induced central nervous system disease. *Nature.* 238:335–337. http://dx.doi.org/10.1038/238335a0

Dalmau, J., and M.R. Rosenfeld. 2008. Paraneoplastic syndromes of the CNS. *Lancet Neurol.* 7:327–340. http://dx.doi.org/10.1016/S1474-4422(08)70060-7

Deb, C., R.G. Lafrance-Corey, L. Zoecklein, L. Papke, M. Rodriguez, and C.L. Howe. 2009. Demyelinated axons and motor function are protected by genetic deletion of perforin in a mouse model of multiple sclerosis. *J. Neuropathol. Exp. Neurol.* 68:1037–1048. http://dx.doi.org/10.1097/NEN.0b013e3181b5417e

Deb, C., R.G. Lafrance-Corey, W.F. Schmalstieg, B.M. Sauer, H. Wang, C.L. German, A.J. Windebank, M. Rodriguez, and C.L. Howe. 2010. CD8+ T cells cause disability and axon loss in a mouse model of multiple sclerosis. *PLoS ONE.* 5:e12478. http://dx.doi.org/10.1371/journal.pone.0012478

Dewachter, I., D. Reversé, N. Caluwaerts, L. Ris, C. Kuipéri, C. Van den Haute, K. Spittaels, L. Umans, L. Serneels, E. Thiry, et al. 2002. Neuronal deficiency of presenilin 1 inhibits amyloid plaque formation and corrects hippocampal long-term potentiation but not a cognitive defect of amyloid precursor protein [V717I] transgenic mice. *J. Neurosci.* 22:3445–3453.

Dutta, R., J. McDonough, X. Yin, J. Peterson, A. Chang, T. Torres, T. Gudz, W.B. Macklin, D.A. Lewis, R.J. Fox, et al. 2006. Mitochondrial dysfunction as a cause of axonal degeneration in multiple sclerosis patients. *Ann. Neurol.* 59:478–489. http://dx.doi.org/10.1002/ana.20736

Emonet, S.F., L. Garidou, D.B. McGavern, and J.C. de la Torre. 2009. Generation of recombinant lymphocytic choriomeningitis viruses with trisegmented genomes stably expressing two additional genes of interest. *Proc. Natl. Acad. Sci. USA.* 106:3473–3478. http://dx.doi.org/10.1073/pnas.0900088106

Farrell, M.A., L. Cheng, M.E. Cornford, W.W. Grody, and H.V. Vinters. 1991. Cytomegalovirus and Rasmussen's encephalitis. *Lancet.* 337:1551–1552. http://dx.doi.org/10.1016/0140-6736(91)93249-9

Feng, G., R.H. Mellor, M. Bernstein, C. Keller-Peck, Q.T. Nguyen, M. Wallace, J.M. Nerbonne, J.W. Lichtman, and J.R. Sanes. 2000. Imaging neuronal subsets in transgenic mice expressing multiple spectral variants of GFP. *Neuron.* 28:41–51. http://dx.doi.org/10.1016/S0896-6273(00)00084-2

Friedman, H., L. Ch'ien, and D. Parham. 1977. Virus in brain of child with hemiplegia, hemiconvulsions, and epilepsy. *Lancet.* 2:666. http://dx.doi.org/10.1016/S0140-6736(77)92540-5

Friese, M.A., and L. Fugger. 2005. Autoreactive CD8+ T cells in multiple sclerosis: a new target for therapy? *Brain.* 128:1747–1763. http://dx.doi.org/10.1093/brain/awh578

Garin, N., and G. Escher. 2001. The development of inhibitory synaptic specializations in the mouse deep cerebellar nuclei. *Neuroscience.* 105:431–441. http://dx.doi.org/10.1016/S0306-4522(01)00127-0

Gilmore, C.P., I. Donaldson, L. Bö, T. Owens, J. Lowe, and N. Evangelou. 2009. Regional variations in the extent and pattern of grey matter demyelination in multiple sclerosis: a comparison between the cerebral cortex, cerebellar cortex, deep grey matter nuclei and the spinal cord. *J. Neurol. Neurosurg. Psychiatry.* 80:182–187. http://dx.doi.org/10.1136/jnnp.2008.148767

Goverman, J. 2009. Autoimmune T cell responses in the central nervous system. *Nat. Rev. Immunol.* 9:393–407. http://dx.doi.org/10.1038/nri2550

Guidotti, L.G., T. Ishikawa, M.V. Hobbs, B. Matzke, R. Schreiber, and F.V. Chisari. 1996. Intracellular inactivation of the hepatitis B virus by cytotoxic T lymphocytes. *Immunity.* 4:25–36. http://dx.doi.org/10.1016/S1074-7613(00)80295-2

Hauser, S.L., A.K. Bhan, F. Gilles, M. Kemp, C. Kerr, and H.L. Weiner. 1986. Immunohistochemical analysis of the cellular infiltrate in multiple sclerosis lesions. *Ann. Neurol.* 19:578–587. http://dx.doi.org/10.1002/ana.410190610

Hommes, D.W., T.L. Mikhajlova, S. Stoinov, D. Stimac, B. Vucelic, J. Lonovics, M. Zákuciová, G. D'Haens, G. Van Assche, S. Ba, et al. 2006. Fontolizumab, a humanised anti-interferon gamma antibody, demonstrates safety and clinical activity in patients with moderate to severe Crohn's disease. *Gut.* 55:1131–1137. http://dx.doi.org/10.1136/gut.2005.079392

Huang, S., W. Hendriks, A. Althage, S. Hemmi, H. Bluethmann, R. Kamijo, J. Vilcek, R.M. Zinkernagel, and M. Aguet. 1993. Immune response in mice that lack the interferon-gamma receptor. *Science.* 259:1742–1745. http://dx.doi.org/10.1126/science.8456301

Johnson, G.V., and R.S. Jope. 1992. The role of microtubule-associated protein 2 (MAP-2) in neuronal growth, plasticity, and degeneration. *J. Neurosci. Res.* 33:505–512. http://dx.doi.org/10.1002/jnr.490330402

Joly, E., and M.B. Oldstone. 1992. Neuronal cells are deficient in loading peptides onto MHC class I molecules. *Neuron.* 8:1185–1190. http://dx.doi.org/10.1016/0896-6273(92)90138-4

Joly, E., L. Mucke, and M.B. Oldstone. 1991. Viral persistence in neurons explained by lack of major histocompatibility class I expression. *Science.* 253:1283–1285. http://dx.doi.org/10.1126/science.1891717

Kägi, D., B. Ledermann, K. Bürki, P. Seiler, B. Odermatt, K.J. Olsen, E.R. Podack, R.M. Zinkernagel, and H. Hengartner. 1994. Cytotoxicity mediated by T cells and natural killer cells is greatly impaired in perforin-deficient mice. *Nature.* 369:31–37. http://dx.doi.org/10.1038/369031a0

Kägi, D., B. Odermatt, P.S. Ohashi, R.M. Zinkernagel, and H. Hengartner. 1996. Development of insulitis without diabetes in transgenic mice lacking perforin-dependent cytotoxicity. *J. Exp. Med.* 183:2143–2152. http://dx.doi.org/10.1084/jem.183.5.2143

Kallmann, B.A., V. Hummel, T. Lindenlaub, K. Ruprecht, K.V. Toyka, and P. Rieckmann. 2000. Cytokine-induced modulation of cellular adhesion to human cerebral endothelial cells is mediated by soluble vascular cell adhesion molecule-1. *Brain*. 123:687–697. http://dx.doi.org/10.1093/brain/123.4.687

Khanna, K.M., R.H. Bonneau, P.R. Kinchington, and R.L. Hendricks. 2003. Herpes simplex virus-specific memory CD8+ T cells are selectively activated and retained in latently infected sensory ganglia. *Immunity*. 18:593–603. http://dx.doi.org/10.1016/S1074-7613(03)00112-2

Kim, E.Y., J.J. Priatel, S.J. Teh, and H.S. Teh. 2006. TNF receptor type 2 (p75) functions as a costimulator for antigen-driven T cell responses in vivo. *J. Immunol.* 176:1026–1035.

Kim, I.J., H.N. Beck, P.J. Lein, and D. Higgins. 2002. Interferon gamma induces retrograde dendritic retraction and inhibits synapse formation. *J. Neurosci.* 22:4530–4539.

Li, Y., A. Uccelli, K.D. Laxer, M.C. Jeong, H.V. Vinters, W.W. Tourtellotte, S.L. Hauser, and J.R. Oksenberg. 1997. Local-clonal expansion of infiltrating T lymphocytes in chronic encephalitis of Rasmussen. *J. Immunol.* 158:1428–1437.

Lin, W., A. Kemper, J.L. Dupree, H.P. Harding, D. Ron, and B. Popko. 2006. Interferon-gamma inhibits central nervous system remyelination through a process modulated by endoplasmic reticulum stress. *Brain*. 129:1306–1318. http://dx.doi.org/10.1093/brain/awl044

Liu, Y., I. Teige, B. Birnir, and S. Issazadeh-Navikas. 2006. Neuron-mediated generation of regulatory T cells from encephalitogenic T cells suppresses EAE. *Nat. Med.* 12:518–525. http://dx.doi.org/10.1038/nm1402

Luche, H., O. Weber, T. Nageswara Rao, C. Blum, and H.J. Fehling. 2007. Faithful activation of an extra-bright red fluorescent protein in "knock-in" Cre-reporter mice ideally suited for lineage tracing studies. *Eur. J. Immunol.* 37:43–53. http://dx.doi.org/10.1002/eji.200636745

Mahad, D.J., I. Ziabreva, G. Campbell, N. Lax, K. White, P.S. Hanson, H. Lassmann, and D.M. Turnbull. 2009. Mitochondrial changes within axons in multiple sclerosis. *Brain*. 132:1161–1174. http://dx.doi.org/10.1093/brain/awp046

Manning, P.T., E.M. Johnson Jr., C.L. Wilcox, M.A. Palmatier, and J.H. Russell. 1987. MHC-specific cytotoxic T lymphocyte killing of dissociated sympathetic neuronal cultures. *Am. J. Pathol.* 128:395–409.

Manrique-Hoyos, N., T. Jürgens, M. Grønborg, M. Kreutzfeldt, M. Schedensack, T. Kuhlmann, C. Schrick, W. Brück, H. Urlaub, M. Simons, and D. Merkler. 2012. Late motor decline after accomplished remyelination: impact for progressive multiple sclerosis. *Ann. Neurol.* 71:227–244. http://dx.doi.org/10.1002/ana.22681

McDole, J.R., S.C. Danzer, R.Y. Pun, Y. Chen, H.L. Johnson, I. Pirko, and A.J. Johnson. 2010. Rapid formation of extended processes and engagement of Theiler's virus-infected neurons by CNS-infiltrating CD8 T cells. *Am. J. Pathol.* 177:1823–1833. http://dx.doi.org/10.2353/ajpath.2010.100231

Medana, I.M., A. Gallimore, A. Oxenius, M.M. Martinic, H. Wekerle, and H. Neumann. 2000. MHC class I-restricted killing of neurons by virus-specific CD8+ T lymphocytes is effected through the Fas/FasL, but not the perforin pathway. *Eur. J. Immunol.* 30:3623–3633. http://dx.doi.org/10.1002/1521-4141(200012)30:12<3623::AID-IMMU3623>3.0.CO;2-F

Medana, I., Z. Li, A. Flügel, J. Tschopp, H. Wekerle, and H. Neumann. 2001a. Fas ligand (CD95L) protects neurons against perforin-mediated T lymphocyte cytotoxicity. *J. Immunol.* 167:674–681.

Medana, I., M.A. Martinic, H. Wekerle, and H. Neumann. 2001b. Transection of major histocompatibility complex class I-induced neurites by cytotoxic T lymphocytes. *Am. J. Pathol.* 159:809–815. http://dx.doi.org/10.1016/S0002-9440(10)61755-5

Merkler, D., E. Horvath, W. Bruck, R.M. Zinkernagel, J.C. Del la Torre, and D.D. Pinschewer. 2006. "Viral déjà vu" elicits organ-specific immune disease independent of reactivity to self. *J. Clin. Invest.* 116:1254–1263. http://dx.doi.org/10.1172/JCI27372

Meuth, S.G., A.M. Herrmann, O.J. Simon, V. Siffrin, N. Melzer, S. Bittner, P. Meuth, H.F. Langer, S. Hallermann, N. Boldakowa, et al. 2009. Cytotoxic CD8+ T cell-neuron interactions: perforin-dependent electrical silencing precedes but is not causally linked to neuronal cell death. *J. Neurosci.* 29:15397–15409. http://dx.doi.org/10.1523/JNEUROSCI.4339-09.2009

Mizuno, T., G. Zhang, H. Takeuchi, J. Kawanokuchi, J. Wang, Y. Sonobe, S. Jin, N. Takada, Y. Komatsu, and A. Suzumura. 2008. Interferon-gamma directly induces neurotoxicity through a neuron specific, calcium-permeable complex of IFN-gamma receptor and AMPA GluR1 receptor. *FASEB J.* 22:1797–1806. http://dx.doi.org/10.1096/fj.07-099499

Murray, P.D., D.B. McGavern, X. Lin, M.K. Njenga, J. Leibowitz, L.R. Pease, and M. Rodriguez. 1998. Perforin-dependent neurologic injury in a viral model of multiple sclerosis. *J. Neurosci.* 18:7306–7314.

Neumann, H., A. Cavalié, D.E. Jenne, and H. Wekerle. 1995. Induction of MHC class I genes in neurons. *Science*. 269:549–552. http://dx.doi.org/10.1126/science.7624779

Neumann, H., H. Schmidt, A. Cavalié, D. Jenne, and H. Wekerle. 1997. Major histocompatibility complex (MHC) class I gene expression in single neurons of the central nervous system: differential regulation by interferon (IFN)-γ and tumor necrosis factor (TNF)-α. *J. Exp. Med.* 185:305–316. http://dx.doi.org/10.1084/jem.185.2.305

Neumann, H., I.M. Medana, J. Bauer, and H. Lassmann. 2002. Cytotoxic T lymphocytes in autoimmune and degenerative CNS diseases. *Trends Neurosci.* 25:313–319. http://dx.doi.org/10.1016/S0166-2236(02)02154-9

Nikić, I., D. Merkler, C. Sorbara, M. Brinkoetter, M. Kreutzfeldt, F.M. Bareyre, W. Brück, D. Bishop, T. Misgeld, and M. Kerschensteiner. 2011. A reversible form of axon damage in experimental autoimmune encephalomyelitis and multiple sclerosis. *Nat. Med.* 17:495–499. http://dx.doi.org/10.1038/nm.2324

Olert, J., K.H. Wiedorn, T. Goldmann, H. Kühl, Y. Mehraein, H. Scherthan, F. Niketeghad, E. Vollmer, A.M. Müller, and J. Müller-Navia. 2001. HOPE fixation: a novel fixing method and paraffin-embedding technique for human soft tissues. *Pathol. Res. Pract.* 197:823–826. http://dx.doi.org/10.1078/0344-0338-00166

Owens, G.C., M.N. Huynh, J.W. Chang, D.L. McArthur, M.J. Hickey, H.V. Vinters, G.W. Mathern, and C.A. Kruse. 2013. Differential expression of interferon-γ and chemokine genes distinguishes Rasmussen encephalitis from cortical dysplasia and provides evidence for an early Th1 immune response. *J. Neuroinflammation*. 10:56. http://dx.doi.org/10.1186/1742-2094-10-56

Panitch, H.S., R.L. Hirsch, J. Schindler, and K.P. Johnson. 1987. Treatment of multiple sclerosis with gamma interferon: exacerbations associated with activation of the immune system. *Neurology*. 37:1097–1102. http://dx.doi.org/10.1212/WNL.37.7.1097

Pardo, C.A., E.P. Vining, L. Guo, R.L. Skolasky, B.S. Carson, and J.M. Freeman. 2004. The pathology of Rasmussen syndrome: stages of cortical involvement and neuropathological studies in 45 hemispherectomies. *Epilepsia*. 45:516–526. http://dx.doi.org/10.1111/j.0013-9580.2004.33103.x

Peschon, J.J., D.S. Torrance, K.L. Stocking, M.B. Glaccum, C. Otten, C.R. Willis, K. Charrier, P.J. Morrissey, C.B. Ware, and K.M. Mohler. 1998. TNF receptor-deficient mice reveal divergent roles for p55 and p75 in several models of inflammation. *J. Immunol.* 160:943–952.

Pinschewer, D.D., L. Flatz, R. Steinborn, E. Horvath, M. Fernandez, H. Lutz, M. Suter, and A. Bergthaler. 2010a. Innate and adaptive immune control of genetically engineered live-attenuated arenavirus vaccine prototypes. *Int. Immunol.* 22:749–756. http://dx.doi.org/10.1093/intimm/dxq061

Pinschewer, D.D., M. Schedensack, A. Bergthaler, E. Horvath, W. Brück, M. Löhning, and D. Merkler. 2010b.T cells can mediate viral clearance from ependyma but not from brain parenchyma in a major histocompatibility class I- and perforin-independent manner. *Brain*. 133:1054–1066. http://dx.doi.org/10.1093/brain/awq028

Pircher, H., K. Bürki, R. Lang, H. Hengartner, and R.M. Zinkernagel. 1989. Tolerance induction in double specific T-cell receptor transgenic mice varies with antigen. *Nature*. 342:559–561. http://dx.doi.org/10.1038/342559a0

Platanias, L.C. 2005. Mechanisms of type-I- and type-II-interferon-mediated signalling. *Nat. Rev. Immunol.* 5:375–386. http://dx.doi.org/10.1038/nri1604

Probst, H.C., K. Tschannen, A. Gallimore, M. Martinic, M. Basler, T. Dumrese, E. Jones, and M.F. van den Broek. 2003. Immunodominance of an antiviral cytotoxic T cell response is shaped by the kinetics of viral protein expression. *J. Immunol.* 171:5415–5422.

Rall, G.F., L. Mucke, and M.B. Oldstone. 1995. Consequences of cytotoxic T lymphocyte interaction with major histocompatibility complex class I–expressing neurons in vivo. *J. Exp. Med.* 182:1201–1212. http://dx.doi.org/10.1084/jem.182.5.1201

Ramana, C.V., M.P. Gil, R.D. Schreiber, and G.R. Stark. 2002. Stat1-dependent and -independent pathways in IFN-gamma-dependent signaling. *Trends Immunol.* 23:96–101. http://dx.doi.org/10.1016/S1471-4906(01)02118-4

Rasmussen, T., J. Olszewski, and D. Lloydsmith. 1958. Focal seizures due to chronic localized encephalitis. *Neurology*. 8:435–445. http://dx.doi.org/10.1212/WNL.8.6.435

Reinisch, W., W. de Villiers, L. Bene, L. Simon, I. Rácz, S. Katz, I. Altorjay, B. Feagan, D. Riff, C.N. Bernstein, et al. 2010. Fontolizumab in moderate to severe Crohn's disease: a phase 2, randomized, double-blind, placebo-controlled, multiple-dose study. *Inflamm. Bowel Dis.* 16:233–242. http://dx.doi.org/10.1002/ibd.21038

Rensing-Ehl, A., U. Malipiero, M. Irmler, J. Tschopp, D. Constam, and A. Fontana. 1996. Neurons induced to express major histocompatibility complex class I antigen are killed via the perforin and not the Fas (APO-1/CD95) pathway. *Eur. J. Immunol.* 26:2271–2274. http://dx.doi.org/10.1002/eji.1830260945

Scheikl, T., B. Pignolet, C. Dalard, S. Desbois, D. Raison, M. Yamazaki, A. Saoudi, J. Bauer, H. Lassmann, H. Hardin-Pouzet, and R.S. Liblau. 2012. Cutting edge: neuronal recognition by CD8 T cells elicits central diabetes insipidus. *J. Immunol.* 188:4731–4735. http://dx.doi.org/10.4049/jimmunol.1102998

Schwab, N., C.G. Bien, A. Waschbisch, A. Becker, G.H. Vince, K. Dornmair, and H. Wiendl. 2009. CD8+ T-cell clones dominate brain infiltrates in Rasmussen encephalitis and persist in the periphery. *Brain*. 132:1236–1246. http://dx.doi.org/10.1093/brain/awp003

Sequiera, L.W., L.C. Jennings, L.H. Carrasco, M.A. Lord, A. Curry, and R.N. Sutton. 1979. Detection of herpes-simplex viral genome in brain tissue. *Lancet*. 2:609–612. http://dx.doi.org/10.1016/S0140-6736(79)91667-2

Shinkai, Y., G. Rathbun, K.P. Lam, E.M. Oltz, V. Stewart, M. Mendelsohn, J. Charron, M. Datta, F. Young, A.M. Stall, et al. 1992. RAG-2-deficient mice lack mature lymphocytes owing to inability to initiate V(D)J rearrangement. *Cell*. 68:855–867. http://dx.doi.org/10.1016/0092-8674(92)90029-C

Shrestha, B., and M.S. Diamond. 2007. Fas ligand interactions contribute to CD8+ T-cell-mediated control of West Nile virus infection in the central nervous system. *J. Virol.* 81:11749–11757. http://dx.doi.org/10.1128/JVI.01136-07

Sobottka, B., M.D. Harrer, U. Ziegler, K. Fischer, H. Wiendl, T. Hünig, B. Becher, and N. Goebels. 2009. Collateral bystander damage by myelin-directed CD8+ T cells causes axonal loss. *Am. J. Pathol.* 175:1160–1166. http://dx.doi.org/10.2353/ajpath.2009.090340

Stinchcombe, J.C., and G.M. Griffiths. 2007. Secretory mechanisms in cell-mediated cytotoxicity. *Annu. Rev. Cell Dev. Biol.* 23:495–517. http://dx.doi.org/10.1146/annurev.cellbio.23.090506.123521

ter Meulen, V., M.J. Carter, H. Wege, and R. Watanabe. 1984. Mechanisms and consequences of virus persistence in the human nervous system. *Ann. N. Y. Acad. Sci.* 436:86–97. http://dx.doi.org/10.1111/j.1749-6632.1984.tb14778.x

Walter, G.F., and R.R. Renella. 1989. Epstein-Barr virus in brain and Rasmussen's encephalitis. *Lancet*. 1:279–280. http://dx.doi.org/10.1016/S0140-6736(89)91292-0

Watanabe-Fukunaga, R., C.I. Brannan, N.G. Copeland, N.A. Jenkins, and S. Nagata. 1992. Lymphoproliferation disorder in mice explained by defects in Fas antigen that mediates apoptosis. *Nature*. 356:314–317. http://dx.doi.org/10.1038/356314a0

Whitmire, J.K., J.T. Tan, and J.L. Whitton. 2005. Interferon-γ acts directly on $CD8^+$ T cells to increase their abundance during virus infection. *J. Exp. Med.* 201:1053–1059. http://dx.doi.org/10.1084/jem.20041463

Zhang, S., J. Boyd, K. Delaney, and T.H. Murphy. 2005. Rapid reversible changes in dendritic spine structure in vivo gated by the degree of ischemia. *J. Neurosci.* 25:5333–5338. http://dx.doi.org/10.1523/JNEUROSCI.1085-05.2005